Bioorganic Chemistry 141 (2023) 106917

Contents lists available at ScienceDirect

Bioorganic Chemistry

journal homepage: www.elsevier.com/locate/bioorg

Probing naphthalene diimide and 3-hydroxypropylphosphate as end-conjugating moieties for improved thrombin binding aptamers: Structural and biological effects

Claudia Riccardi [a], Kévan Pérez de Carvasal [b], Chiara Platella [a], Albert Meyer [b], Michael Smietana [b], François Morvan [b,*], Daniela Montesarchio [a,*]

[a] Department of Chemical Sciences, University of Naples Federico II, 80126 Naples, Italy
[b] Institut des Biomolécules Max Mousseron, Université de Montpellier, CNRS, ENSCM, 34095 Montpellier, France

ARTICLE INFO

Keywords:
Thrombin binding aptamer
Oligodeoxyribonucleotides
G-quadruplex structures
Conjugation
Naphthalendiimide
3-Hydroxypropylphosphate
Biophysical characterization
Serum resistance evaluation
Anticoagulant activity

ABSTRACT

The limitations associated with the in vivo use of the thrombin binding aptamer (TBA or TBA_{15}) have dramatically stimulated the search of suitable chemically modified analogues in order to discover effective and reversible inhibitors of thrombin activity. In this context, we previously proposed cyclic and pseudo-cyclic TBA analogues with improved stability that proved to be more active than the parent aptamer.

Herein, we have investigated a novel library of TBA derivatives carrying naphthalene diimide (NDI) moieties at the 3′- or 5′-end. In a subset of the investigated oligonucleotides, additional 3-hydroxypropylphosphate (HPP) groups were introduced at one or both ends of the TBA sequence. Evaluation of the G-quadruplex thermal stability, serum nuclease resistance and in vitro anticoagulant activity of the new TBA analogues allowed rationalizing the effect of these appendages on the activity of the aptamer on the basis of their relative position. Notably, most of the different TBA analogues tested were more potent thrombin inhibitors than unmodified TBA. Particularly, the analogue carrying an NDI group at the 5′-end and an HPP group at the 3′-end, named **N-TBA-p**, exhibited enhanced G-quadruplex thermal stability ($\Delta T_m + 14^\circ$ C) and ca. 10-fold improved nuclease resistance in serum compared to the native aptamer. **N-TBA-p** also induced prolonged and dose-dependent clotting times, showing a ca. 11-fold higher anticoagulant activity compared to unmodified TBA, as determined by spectroscopic methods. Overall, **N-TBA-p** proved to be in vitro a more efficient thrombin inhibitor than all the best ones previously investigated in our group. Its interesting features, associated with its easy preparation, make it a very promising candidate for future in vivo studies.

1. Introduction

One of the most investigated oligonucleotide aptamers, claiming the highest number of structural variants thus far proposed, is the 15-mer thrombin binding aptamer, also known as TBA or TBA_{15} (5′-GGTTGGTGTGGTTGG-3′). [1–6] This G-rich aptamer interferes with the coagulation cascade, selectively recognizing the fibrinogen-binding exosite I of thrombin, a multifunctional "trypsin-like" serine protease with a pivotal function in the last step of blood clotting. [7,8] Its biological activity is strictly linked to its peculiar three-dimensional architecture. Indeed, TBA folds into a chair-like, antiparallel, unimolecular G-quadruplex (G4) structure both in the free and protein-bound form. [9–11] Although TBA evidenced a promising pharmacokinetic profile in humans, its preclinical and clinical evaluations were halted after phase I studies due to suboptimal dosing profiles. [12–14] Thus, to improve its biophysical and biological properties and obtain effective anticoagulant agents, a large number of analogues of this G4-forming aptamer have been designed and synthesized. [15]

In this scenario, we recently analyzed a small library of cyclic TBA analogues obtained by covalently connecting its 5′- and 3′- ends with flexible linkers.[16,17] These derivatives exhibited a G4 structure with exceptionally improved thermal stability and nuclease resistance. However, these favorable properties were associated with reduced biological activity, suggesting that higher flexibility in the linker structure was necessary.[16,17]

Further studies were thus devoted to study pseudo-cyclic TBA

* Corresponding authors.
E-mail addresses: francois.morvan@umontpellier.fr (F. Morvan), daniela.montesarchio@unina.it (D. Montesarchio).

https://doi.org/10.1016/j.bioorg.2023.106917
Received 4 September 2023; Received in revised form 27 September 2023; Accepted 9 October 2023
Available online 14 October 2023

analogues, where a cyclic-like structure of this aptamer was obtained not through covalent bonds, but *via* π-π stacking or charge-transfer interactions of different aromatic probes inserted at the oligonucleotide 5′ and 3′ termini.[18]

In detail, TBA analogues were obtained *via* end-conjugation with the electron-rich 1,5-dialkoxy naphthalene (DAN or D) and the electron-deficient 1,8,4,5-naphthalenetetra-carboxylic diimide (NDI or N) motifs, which favored the stabilization of the G4 structure while allowing sufficient flexibility to the aptamer architecture so to ensure both a compact G4 folding and high thrombin recognition. The derivative named **TBA-NNp/DDp**, carrying two charge transfer pairs, proved to be the best candidate in the studied set of compounds, exhibiting a more stable G-quadruplex structure ($\Delta T_m + 11$ and $+ 8$ °C in the selected K^+- and Na^+-rich buffer, respectively), a 4.5-fold increase of nuclease resistance and a 1.2-fold higher anticoagulant activity compared to unmodified TBA.[18]

In this previous study, the TBA analogues conjugated at the 3′-end with an NDI (**TBA-N**) or a DAN (**TBA-D**) moiety were also synthesized as controls. While **TBA-D** showed a lower T_m value ($\Delta T_m - 6$ °C) and only a slight increase in nuclease resistance compared to TBA, **TBA-N** was characterized by a higher T_m value ($\Delta T_m + 13$ °C) and a marked increase of nuclease stability in serum with respect to the parent aptamer. However, their anticoagulant activity was not determined. The high G4 thermal stabilization observed for **TBA-N** is not surprising since it has been reported that NDI[19,20] or perylenetetra-carboxylic diimide (PDI)[21] derivatives are able to stabilize the G-quadruplex structure of TBA.[22]

In our former study, some of the proposed TBA analogues were also decorated with terminal 3-hydroxypropylphosphate (HPP) groups.[18] Surprisingly, their presence had a significant effect on the stability of the G4 structure, resistance to nuclease degradation and anticoagulant activity. As a general rule, the TBA analogues carrying these appendages showed lower T_m values but higher resistance to nuclease and improved anticoagulant activity. However, the exact role of this conjugating group was not identified. A successive crystallographic study did not provide any clues due to the too high flexibility of these terminal groups.[23]

These different observations prompted us to further investigate TBA derivatives carrying differently substituted NDI appendages and functionalized or not with an HPP group. NDI moieties were selected as versatile and functional molecules, which have tunable electronic, charge-transfer and optical properties. NDIs have been extensively studied for their potential use across a wide variety of applications including supramolecular chemistry, sensing, catalysis and host–guest complexes for molecular switching devices.[24–26]

In addition, due to their large aromatic surface, NDI dyes can provide π-π stacking interactions with the adjacent G-quartet of the G-quadruplex structure of the aptamer, thereby stabilizing its overall folding. In the set of new compounds here designed, the HPP group was also added in different positions to verify if its insertion confirmed the benefits observed in the case of the pseudo-cyclic derivatives.

In detail, we have synthesized a small library of TBA analogues carrying an NDI moiety either at the 3′ or 5′-end (**TBA-N** and **N-TBA**) and an HPP group either at the other end (**p-TBA-N** and **N-TBA-p**) or directly attached to the NDI (**TBA-Np** and **pN-TBA**) (Fig. 1). To further investigate the effect of the HPP group, we also prepared the analogue of **TBA-N** with an HPP at each end (**p-TBA-Np**), and **TBA-NC3**, an analogue in which the terminal hydroxyl group was removed. As a control, we also synthesized the TBA derivative carrying an HPP group at both termini (**p-TBA-p**).

2. Results and discussion

2.1. Solid phase synthesis of the TBA analogues and characterization

The designed set of modified oligonucleotides was prepared by automated solid phase synthesis according to standard phosphoramidite

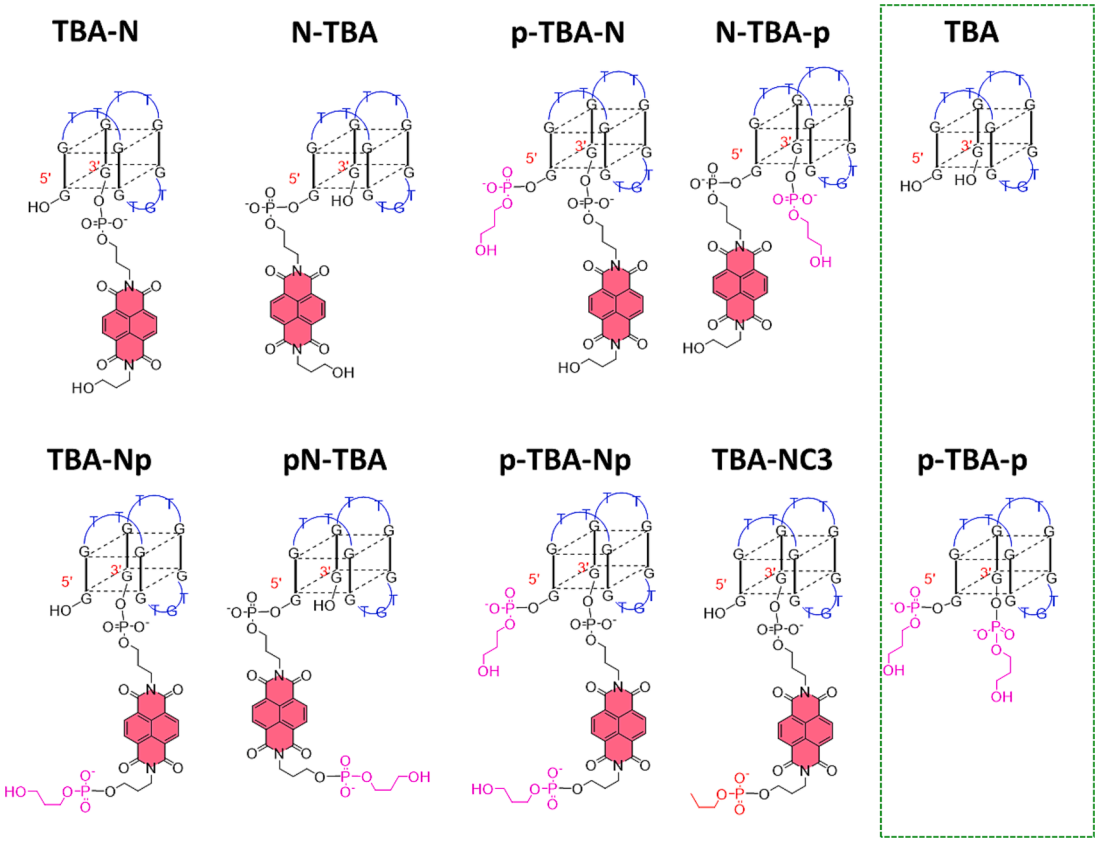

Fig. 1. Chemical structures of the oligonucleotides herein investigated. N = naphthalene diimide; p = 3-hydroxypropylphosphate; C3 = *n*-propyl phosphate.

chemistry using the Q-Linker CPG as the starting solid support and deoxyguanosine phosphoramidite building blocks protected on the nucleobase with the *tert*-butyl phenoxyacetyl group. This combined choice avoids a strong basic treatment in the final deprotection step of the oligonucleotide synthesis that could damage the NDI residue attached at the end of the oligonucleotide chain.

As a representative example, the synthesis of the **p-TBA-Np** analogue is described in detail and reported in Scheme 1. Starting from DMTr-protected 1,3-propanediol-functionalized solid support **1**, the NDI-containing phosphoramidite **2**[27,28] was used in the first coupling step. Then, the assembly of the TBA sequence d(GGTTGGTGTGGTTGG) was realized, followed by a final coupling with DMTr-protected 1,3-propanediol phosphoramidite **3**. After detritylation (using 3 % TCA), treatment with methanolic ammonia allowed the release in solution of **p-TBA-Np**, which was analyzed and purified by RP-HPLC and characterized by MALDI-TOF mass spectrometry. The other TBA analogues were synthesized following similar procedures starting from ad hoc functionalized solid supports (**1**, **4** or dG-CPG), as indicated in Schemes 2-4.

The preparation of **TBA-NC3** required the use of the 2,2′-thiodiethanol-functionalized solid support **5**[29] allowing the release of the oligonucleotide from the solid support by a simple treatment with hot water, finally affording the desired *n*-propyl-phosphodiester moiety at the 3′-end of the target sequence. In this synthetic scheme, the NDI-containing *n*-propyl-phosphoramidite **6** (see Supporting Information for details on its synthesis and characterization) was coupled as the first building block on the solid support and then the TBA sequence was elongated. After detritylation, the final oligonucleotide deprotection involved the following steps: treatment with methanolic ammonia, then solvent evaporation and finally treatment with hot water (60 °C) for 1 h, thus affording the desired **TBA-NC3** (Scheme 5).

All modified oligonucleotides were then purified by HPLC and their identity confirmed by MALDI-TOF analysis. To further check the purity of the synthesized oligonucleotides, a 20 % denaturing PAGE analysis was carried out, using unmodified TBA as reference (Fig. S1). Under the explored conditions, all the TBA analogues migrated as a single band on the gel, showing slightly different electrophoretic mobility properties reflecting their different mass/charge ratios.

2.2. Conformational and spectroscopic properties of the TBA analogues

The spectroscopic properties and conformational behavior of the modified TBA derivatives were studied by UV and CD spectroscopy – always using unmodified TBA as reference – in two different phosphate buffer solutions, containing a high content of K^+ (here indicated as K^+-rich buffer) or of Na^+ (Na^+-rich buffer, i.e. PBS) ions, respectively mimicking the composition of the intra- and extracellular media (see experimental part for details). Indeed, it has been demonstrated that buffer composition, and especially ion concentration, play a key role in G-quadruplex folding also influencing the biophysical[10,30] and biological properties of TBA and its analogues.[30–33]

2.2.1. UV spectroscopy analysis: UV spectra and UV thermal denaturation/renaturation measurements

UV–vis absorption spectra of the TBA derivatives, recorded in H_2O at r.t. (Fig. S2), showed the peculiar absorption features of TBA – with the double-hump band between 230 and 300 nm[16] – and of the NDI probe with contribution in the 300–600 nm region, in accordance with previous studies.[18] With the exception of **p-TBA-p**, not carrying the NDI appendage, all the other sequences conjugated with the NDI moieties exhibited relevant absorption bands centered at 364 and 386 nm, due to π/π^* transitions, similarly to **TBA-N** (grey line, Fig. S2).

UV spectra were then recorded in the selected K^+- and Na^+-rich buffers at low and high temperatures (i.e., 15 and 90 °C) using a 2 μM oligonucleotide concentration. The UV thermal difference spectra (TDS, Fig. 2a,b), representing a "fingerprint" of a specific nucleic acid structure,[34–37] were then determined.

In both saline conditions, all the TBA analogues showed normalized TDS profiles with two positive (at ca. 240 and 275 nm) and two negative bands (around 260 and 295 nm), which are very similar to those found for unmodified TBA (black line, Fig. 2a,b) and diagnostic of the presence in solution of a G-quadruplex structure.[34–37]

In addition, an estimation of the predominant G-quadruplex conformation in solution was obtained by determining the three TDS factors, i.e. $\Delta A_{240}/\Delta A_{295}$, $\Delta A_{255}/\Delta A_{295}$ and $\Delta A_{275}/\Delta A_{295}$. The results indicated values lower than 2, 1.5 and 2, respectively (Table S1), all consistent with the antiparallel G-quadruplex topology,[36] typical of unmodified TBA.

These results demonstrated that the conjugation with the NDI and/or HPP groups had no relevant impact on the overall antiparallel G-quadruplex folding of TBA regardless of whether they were introduced at only one end or at both ends of the TBA sequence.

Then, to study the thermal stability of the G-quadruplex structures formed by the TBA analogues, UV thermal denaturation/renaturation

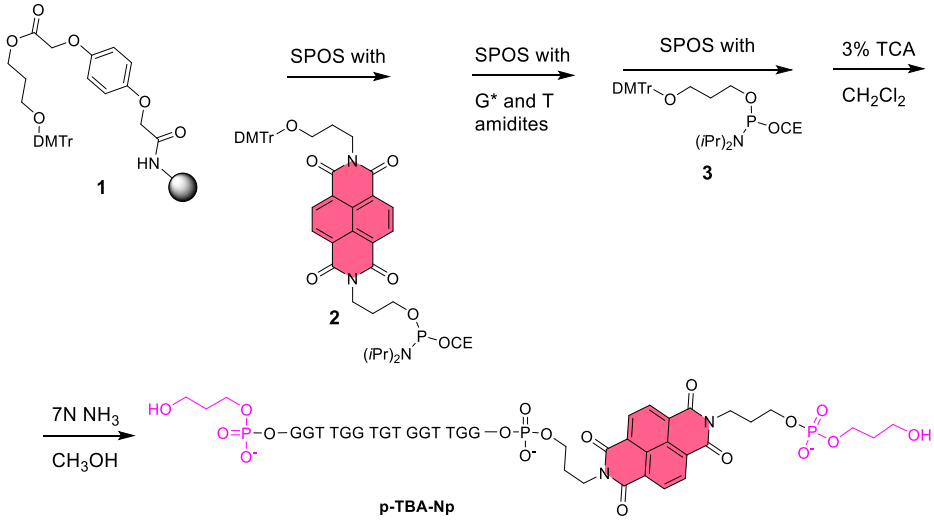

Scheme 1. Solid-supported synthesis of **p-TBA-Np**. DMTr = 4,4′-dimethoxytriphenylmethyl; SPOS: solid phase oligonucleotide synthesis; G* = 5′-*O*-(4,4′-dimethoxytriphenylmethyl)–N^2-*p-tert*-butyl-phenoxyacetyl-2′-deoxyguanosine,3′-*O*-[(2-cyanoethyl)-(*N*,*N*-diisopropyl)]-phosphoramidite; T = 5′- *O*-(4,4′-dimethoxytriphenylmethyl)-thymidine,3′-*O*-[(2-cyanoethyl)-(*N*,*N*-diisopropyl)]-phosphoramidite; TCA = trichloroacetic acid; CE = 2-cyanoethyl; *i*Pr = isopropyl.

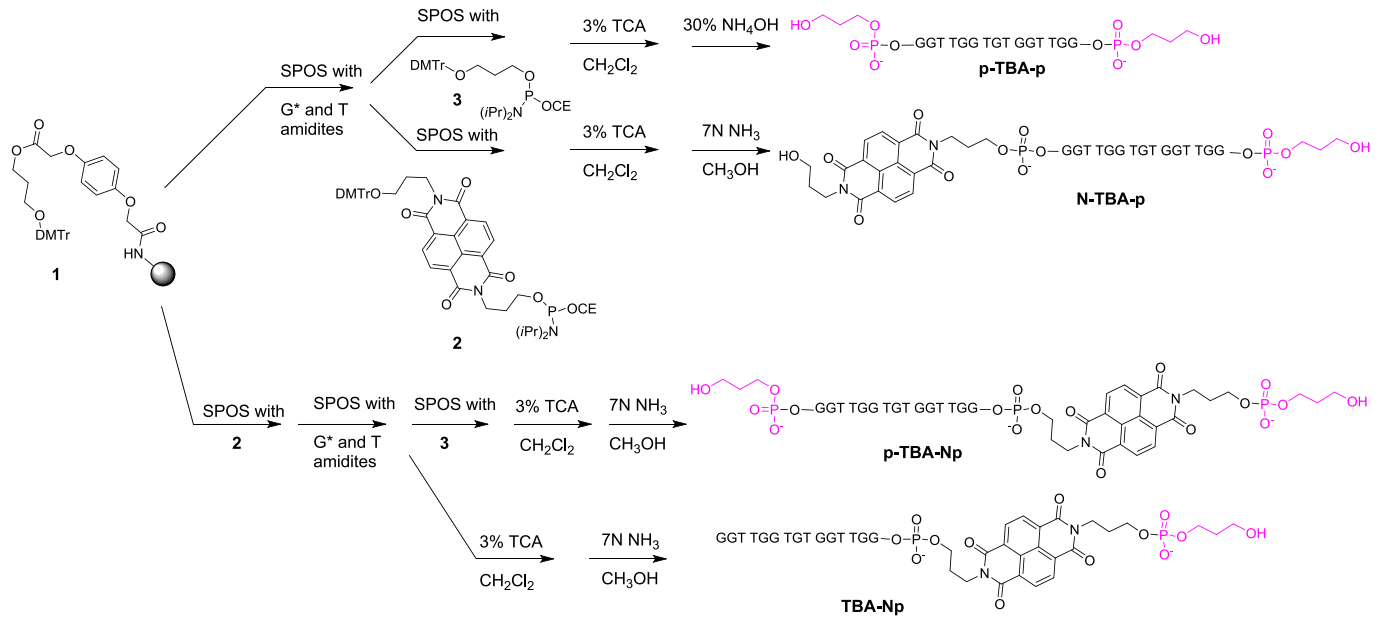

Scheme 2. Solid-supported synthesis of **p-TBA-p**, **N-TBA-p**, **p-TBA-Np** and **TBA-Np**.

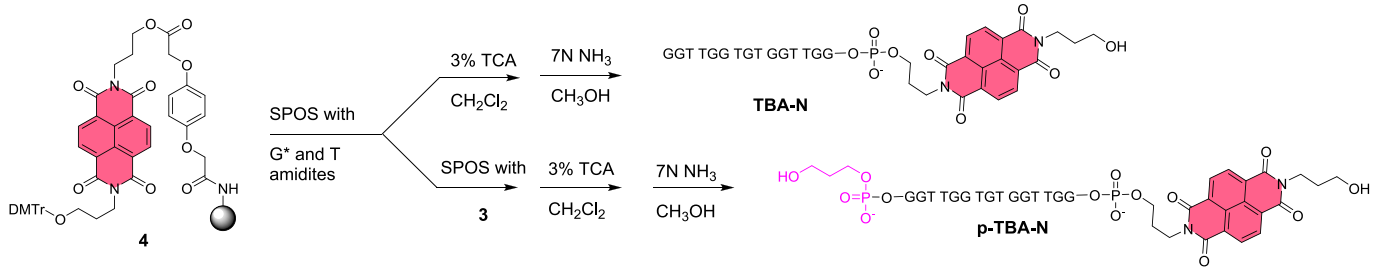

Scheme 3. Solid-supported synthesis of **TBA-N** and **p-TBA-N.**

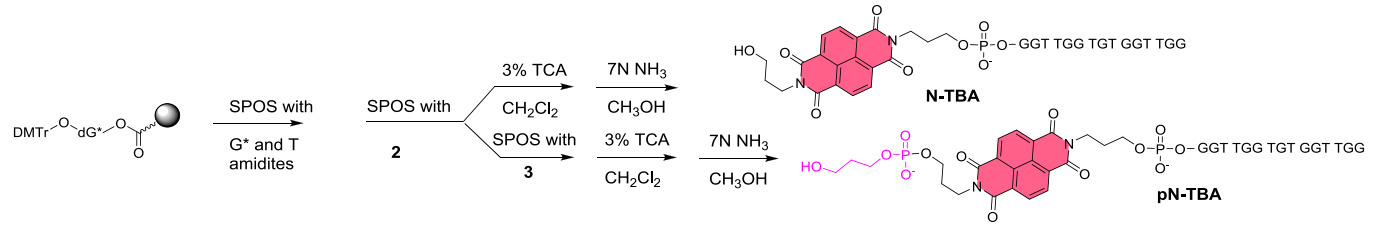

Scheme 4. Solid-supported synthesis of **N-TBA** and **pN-TBA**.

experiments were performed at 2 μM oligonucleotide concentration monitoring the UV signal at 295 nm. The overlapped UV-melting profiles in the 15–90 °C range of all the studied oligonucleotides were reported in terms of normalized absorbance as a function of the temperature in Fig. 2c,d, whereas the overlapped UV-monitored heating/cooling curves for each compound were shown in Figs. S3-S12. All the apparent T_m values obtained from these UV analyses were reported in Table S2.

In all cases, a sigmoidal decrease of the absorbance at 295 nm was found upon increasing the temperature in both K^+- and Na^+-rich buffers (Fig. 2c,d), in agreement with the well-described unfolding process of a G-quadruplex structure.[37–39]

In almost all cases, the UV analysis showed superimposable melting/cooling profiles, indicating that under the experimental conditions tested (scan rate = 1 °C/min), the related denaturation/renaturation processes were essentially reversible. Only few exceptions to this general trend were observed, with a slight hysteresis in the case of **p-TBA-p** in K^+ buffer (Fig. S5a) and **TBA-Np, TBA-NC3, *N*-TBA** and ***N*-TBA-p** in the Na^+-rich solution (Fig. S7b, S9b, S10b and S12b).

In detail, in the K^+-rich buffer, all TBA analogues – except **p-TBA-p, p-TBA-N** and **p-TBA-Np** – revealed a remarkably increased thermal stability compared to unmodified TBA (Fig. 2c), indicating the formation of very stable G4 structures, and particularly in the case of **TBA-N**, **N-TBA** and **N-TBA-p**. In fact, the latter analogues showed apparent T_m values respectively of 56, 56 and 55 °C, corresponding to ΔT_m of + 9, +9 and + 8 compared to the unmodified TBA. Slightly improved T_m values of 53, 53 and 51 °C, with ΔT_m of + 6, +6 and + 4 °C, were respectively found for **TBA-Np, TBA-NC3** and **pN-TBA**. Conversely, UV analysis on **p-TBA-p, p-TBA-N** and **p-TBA-Np** analogues indicated a slight destabilization of their G4 structures with T_m values respectively of 44, 44 and 42 °C, i.e. 3 and 5 °C lower than the native aptamer (Figs. S3-S12 and Table S2).

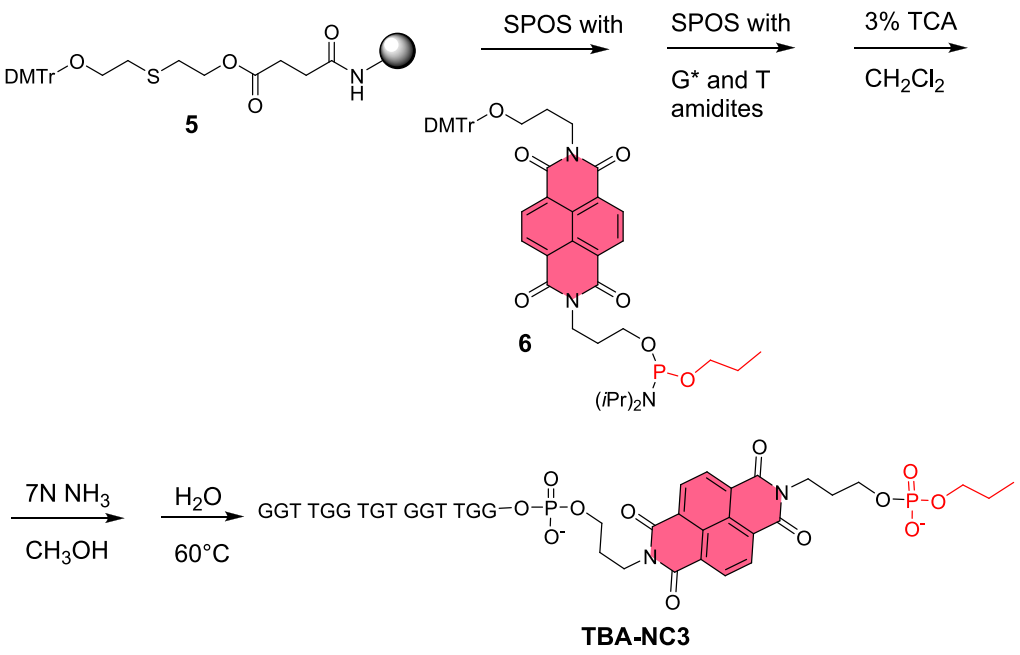

Scheme 5. Solid-supported synthesis of **TBA-NC3.**

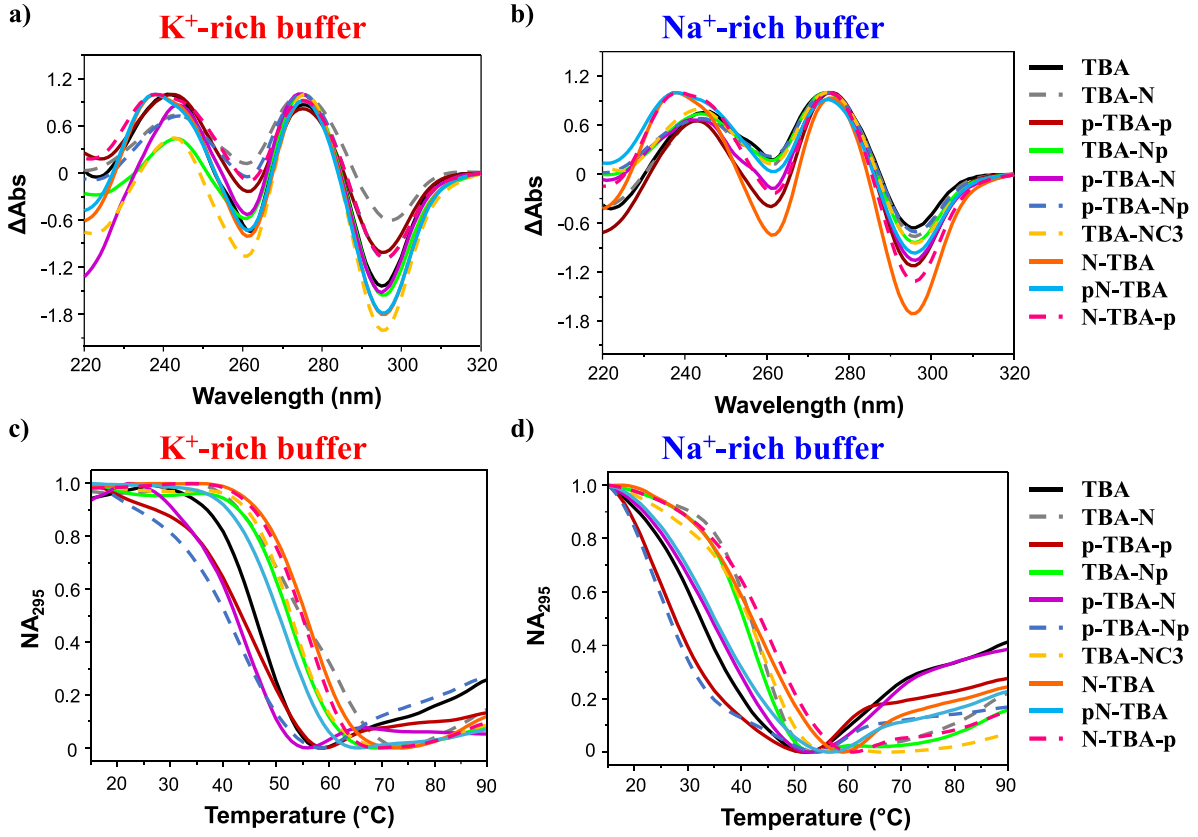

Fig. 2. *UV analysis.* **(a, b)** Representative normalized TDS profiles of the TBA analogues at 2 μM concentration in both the selected K^+- (**a**) and Na^+-rich (**b**) buffer solutions, in comparison with unmodified TBA (black line). TDS profiles are obtained for each aptamer from the subtraction of its UV spectrum registered at 15 °C from the 90 °C one. **(c, d)** Representative UV-melting profiles of the TBA analogues at 2 μM concentration in both the selected K^+- (**c**) and Na^+-rich (**d**) buffer solutions in comparison with unmodified TBA (black line). UV-melting profiles – recorded at 295 nm using a scan rate of 1 °C/min – are reported in terms of normalized absorbance as a function of the temperature.

In turn, in the Na^+-rich buffer, all TBA analogues – except **p-TBA-p** and **p-TBA-Np** – showed an increased thermal stability compared to their parent aptamer (Fig. 2d). The most stabilized G4 structures were those of **N-TBA-p, TBA-NC3**, **N-TBA, TBA-N** and **TBA-Np**, which exhibited apparent T_m values respectively of 45, 44, 44, 43 and 42 °C, corresponding to ΔT_m values of + 13, +12, +12, +11 and + 10 °C,

respectively. In contrast, for **p-TBA-N** and **pN-TBA** T_m values of 35 °C were found, with a ΔTm of + 3 °C, i.e. only slightly improved compared to TBA. Finally, **p-TBA-p** and **p-TBA-Np** formed destabilized G4 structures compared to unmodified TBA, both with T_m values of 25 °C, i.e. 7 °C lower than the native aptamer (Figs. S3-S12 and Table S2).

Overall, the UV-derived T_m values revealed this stability trend: **TBA-N** ≈ **N-TBA** > **N-TBA-p** > **TBA-Np** ≈ **TBA-NC3** > **pN-TBA** > TBA > **p-TBA-N** ≈ **p-TBA-p** > **p-TBA-Np** in the K^+-rich buffer, and ***N*-TBA-p** > **N-TBA** ≈ **TBA-NC3** > **TBA-N** > **TBA-Np** > **p-TBA-N** ≈ **pN-TBA** > TBA > **p-TBA-p** ≈ **p-TBA-Np** in the Na^+-rich buffer solution (Table S2), with data in accordance with the general finding that G4 structures are more stable in K^+- than in Na^+-rich solutions.[40–42]

The bis-conjugation of TBA with HPP groups has a moderate effect on the T_m values (**p-TBA-p** vs. **TBA**: ΔT_m = -3 °C). However, for the TBA analogues bearing an NDI moiety, the position of this additional group has a significant effect on the overall G4 stability (Table S2). Indeed, in the K^+-rich buffer, its direct introduction at the 5′-end induced a strong destabilization (**TBA-N** vs. **p-TBA-N** ΔT_m = -12 °C and **TBA-Np** vs. **p-TBA-Np** ΔT_m = -11 °C) whereas when added at the 3′ extremity no significant effect was observed (**N-TBA** vs. **N-TBA-p** ΔT_m = -1 °C). This destabilization is limited when there is already an NDI at the 5′-end (***N*-TBA** vs. **pN-TBA** ΔT_m = -5 °C) or at the 3′-end (**TBA-N** vs. **TBA-Np** ΔT_m = -3°C). The presence or not of a hydroxyl at the end has not relevant impact (**TBA-Np** ≈ **TBA-NC3**).

In Na^+-rich buffer, a similar behavior was found, with no significant effect upon insertion of the HPP group at the 3′-end (**TBA-N** vs. **TBA-Np** ΔT_m **−1 °C**), and a dramatic destabilization if introduced at the 5′-end (**TBA-N** vs. **p-TBA-N** ΔT_m = -8 °C and **TBA-Np** vs. **p-TBA-Np** ΔT_m −17 °C) (Table S2).

2.2.2. *CD spectroscopy analysis: CD spectra and CD thermal denaturation/renaturation measurements*

In order to deeply investigate the effect of the NDI and HPP appendages on the conformational properties of the studied aptamers, also CD spectra of the TBA analogues were acquired at 15 °C and 2 μM oligonucleotide concentration (Fig. 3a,b). In both the tested saline solutions, all the modified TBA derivatives showed CD spectra essentially superimposable to that of the unmodified aptamer (Fig. 3, black line) having two positive bands, with maxima at about 295 and 247 nm, and one negative band with a minimum at ca. 268 nm. These spectral features are fully consistent with the peculiar antiparallel G4 topology of TBA.[36,42–49]

As expected, for all TBA analogues, positive CD bands showed higher molar ellipticities in K^+ than in Na^+-rich buffer (Fig. 3a,b).[41,42]

More marked differences in the behavior of the TBA analogues were found by comparing their CD-thermal denaturation/renaturation curves, monitoring the intensity of the CD signal at 295 nm on varying the temperature in the 15–90 °C range. The overlapped CD-melting profiles of all the studied oligonucleotides were reported in terms of folded fraction as a function of the temperature in Fig. 3c,d. The

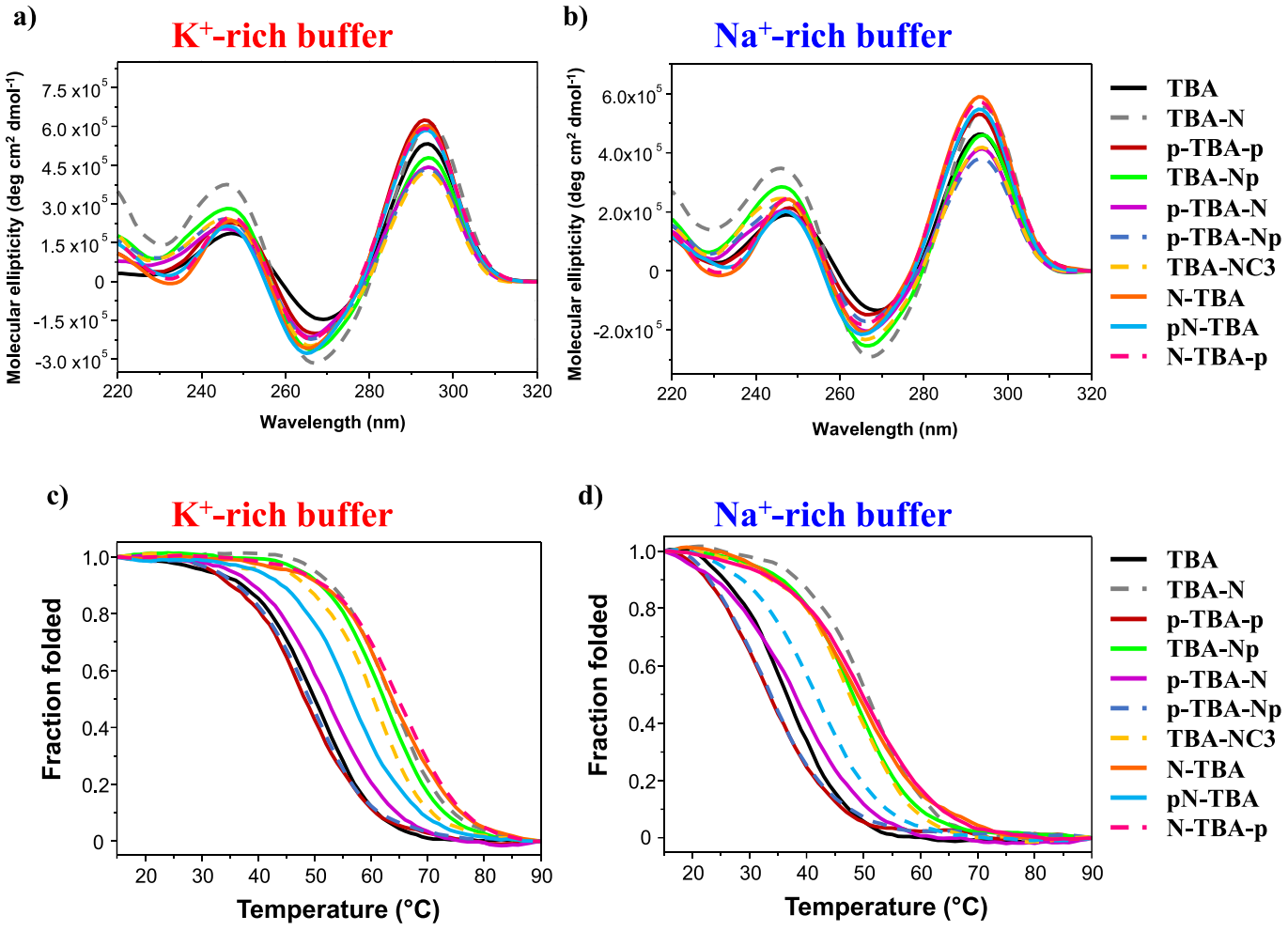

Fig. 3. *CD analysis.* **(a, b)** Representative overlapped CD spectra of the TBA analogues at 2 μM concentration and 15 °C in both the selected K^+- (**a**) and Na^+-rich (**b**) buffer solutions in comparison with unmodified TBA (black line). **(c, d)** Representative overlapped CD-melting profiles of the TBA analogues at 2 μM concentration in both the selected K^+- (**c**) and Na^+-rich (**d**) buffer in comparison with unmodified TBA (black line). CD-melting profiles were recorded following the signal at 295 nm in the 15–90 °C range using a scan rate of 1 °C/min and are reported as folded fraction of each oligonucleotide system as a function of temperature.

overlapped CD-melting/cooling curves for each compound were shown in Figs. S13-S22, while the superimposition of the spectra recorded at 5 °C steps during each heating and cooling experiment were reported in Figs. S23-S32. An overview of the apparent T_m values derived by CD-monitored thermal denaturation/renaturation measurements was reported in Table S3.

In both saline conditions, CD results reinforced the previously described UV data showing similar trends in G4 stability (Fig. 3c,d and Table S3, see the Supporting Information for details).

Overall, CD results were fully consistent with UV analysis outcomes, further confirming that the insertion of HPP groups at both TBA extremities was detrimental for the thermal stability of the G-quadruplex structure compared to the parent aptamer. In contrast, the NDI moiety significantly improved the thermal stability of unmodified TBA, no matter if it was inserted at the 5′ or 3′ end. In turn, the presence of a single HPP group produced different effects depending on its specific position: in general, its insertion at the 5′-end led to a marked destabilization, while its addition at the 3′-end had no dramatic effects or led only to a slight destabilization of the TBA G-quadruplex.

The CD analysis revealed in all cases consistent sigmoidal profiles (Figs. S13-S22), however with a small hysteresis detected between the heating and cooling profiles (differently from TBA and **TBA-N**, Figs. S13 and S14 respectively), thereby indicating that, under the experimental conditions used, the related denaturation/renaturation processes were not perfectly reversible.

During each melting and cooling measurement, CD spectra were also recorded in 5 °C steps (Figs. S23-S32) showing a detectable and progressive reduction of the main CD bands on increasing the temperature during the heating experiment, which was completely reverted upon cooling. This behavior suggested that all TBA analogues were conformationally similar to their parent aptamer from a qualitative point of view. Noteworthy, in both the explored saline conditions, all these derivatives were fully unfolded at 90 °C and completely recovered their peculiar spectral features at 15 °C after the heating/cooling cycle (Figs. S23-S32), confirming the essential, even if not perfect, reversibility of these processes. In particular, as for unmodified TBA, overlapping the CD spectra recorded every 5 °C during each thermal experiment, the diagnostic isodichroic point at ca. 280 nm (Figs. S23-S32) – consistent with a two-state process – was detected.[50–52]

Thus, aiming at disclosing the thermodynamic parameters associated with the G-quadruplex unfolding, the CD-melting data of all the modified TBAs were also treated according to the van't Hoff analysis, based on a 'two-state process' hypothesis.[35,53,54] The standard enthalpy and entropy change values here obtained for unmodified TBA in both the selected saline conditions were in good agreement with those reported in the literature under similar experimental conditions (Table S4).[16,17,55–57]

Inspection of Table S4 revealed that for all the examined TBA derivatives, aptamer folding is an enthalpy-driven process and the obtained ΔH^0 values are consistent with a G-quadruplex structure formed by two G-tetrads, as found for their parent aptamer.[58–61] With the exception of **TBA-N, TBA-Np** and **TBA-NC3**, in both saline conditions, all TBA analogues are characterized by standard enthalpy and entropy changes lower in absolute values compared to unmodified TBA. The higher stability of **TBA-N** and the **TBA-Np** and **TBA-NC3** variants (Table S4) with respect to native TBA is mainly due to the enthalpic factor, suggesting that, upon G-quadruplex folding, additional interactions were established, expectedly by end-stacking of the NDI probe on the adjacent G-tetrad, as typically observed for this kind of ligands in their interaction with G4 structures.[26]

Where observed, the enhanced stability of the NDI-containing TBA analogues with respect to their natural counterpart can be essentially attributed to a favorable ΔS^0 change, which balances the unfavorable ΔH^0 change (Table S4), similarly to what we previously observed for the cyclic[16,17] and pseudo-cyclic TBA derivatives.[18] Overall, the whole set of thermodynamic parameters is fully consistent with the CD-derived T_m values.

2.2.3. Non-denaturing polyacrylamide gel electrophoresis

Polyacrylamide gel electrophoresis (PAGE) experiments under non-denaturing conditions are useful analyses for the study of G4 structures, allowing to determine the molecularity of selected nucleic acids and their ability to form or not aggregates or superstructures in solution.[62–64] Therefore, a native 15 % PAGE analysis was carried out (Fig. 4) on the TBA analogues in comparison with the native aptamer. In both the explored saline conditions, all these oligonucleotides proved to preserve the monomolecular G4 structure typical of their parent aptamer, always appearing as a single band on the gel without any additional retarded species (Fig. 4).

Notably, **p-TBA-Np** in both buffers and **pN-TBA** in Na^+-rich buffer migrated slightly slower than the native aptamer, while **N-TBA-p**, **TBA-Np**, **TBA-NC3** and **N-TBA** migrated slightly faster. Considering that the migration ability of G-quadruplex structures with the same or similar mass/charge ratio on a gel running under native conditions is essentially influenced by their conformation and compactness, PAGE results suggest a slightly more compact G4 structure with respect to unmodified TBA for **TBA-Np**, **TBA-NC3, N-TBA** and **N-TBA-p** (Fig. 4).

2.2.4. Nuclease stability assays

For their potential in vivo use, aptamers have to be sufficiently stable to nuclease degradation in serum, which could deactivate a selected oligonucleotide before it exerts its action. In this frame, it is well-proved that the derivatization of the TBA at the 3′- or 5′-OH extremities with selected appendages can prevent exonuclease digestion.[15–18,65–68] In order to verify if NDI and/or HPP groups conjugation effectively improved the nuclease resistance of the current TBA analogues with respect to the native aptamer, all these oligonucleotides were incubated in fetal bovine serum (FBS) and their fate was monitored by gel electrophoresis. In detail, all the aptamers were first dissolved and annealed in the selected Na^+-rich buffer (i.e., PBS); then, in parallel experiments, each oligonucleotide was incubated in 80 % FBS at 37 °C and monitored for 24 h. At fixed times, aliquots of these aptamer/FBS mixtures were taken, complemented with formamide to block the nuclease degradation and then loaded on the gel under denaturing conditions (Fig. 5). The intensity of each oligonucleotide band on the gel at the distinct investigated time points was then quantified (see experimental part) and reported as normalized percentage with respect to that of the untreated oligonucleotide (time zero, i.e. the same aptamer amount dissolved in PBS). Then, the determined remaining aptamer percentages were fitted using an equation for first order kinetics allowing to estimate for each aptamer its half-life ($t_{1/2}$) value, i.e. the time at which the oligonucleotide amount was 50 % of the initial untreated one. Percentages of remaining aptamer at different incubation time along with the corresponding fitting curves were represented for each oligonucleotide in Fig. S33.

Under the same experimental conditions, all the tested oligonucleotides showed a progressive decrease of the intensity of intact oligonucleotide band, which completely disappeared at different times depending on the specific derivative (Fig. 5). Unmodified TBA completely disappeared in ca. 2 h, exhibiting a $t_{1/2}$ value of 0.6 h. With the exception of **N-TBA** and **pN-TBA**, all the TBA analogues proved to be more resistant in serum than the parent aptamer, even if to a different extent.

In detail, after 7 h FBS incubation, **TBA-N**, **TBA-Np**, **TBA-NC3** and **N-TBA-p** were still detectable, proving to be completely degraded within 24 h (Fig. 5). They exhibited improved $t_{1/2}$ values compared to the unmodified aptamer by a factor of ca. 10.0, 10.5, 8.2 and 9.7-folds respectively, proving to be the most resistant oligonucleotides to nuclease degradation in this series. Slightly visible after a 7 h FBS treatment were the bands of **p-TBA-p**, **p-TBA-N** and **p-TBA-Np** analogues, which showed 2.3-, 3.1- and 3.5-folds higher $t_{1/2}$ values with respect to unmodified TBA, with a moderate increase in nuclease

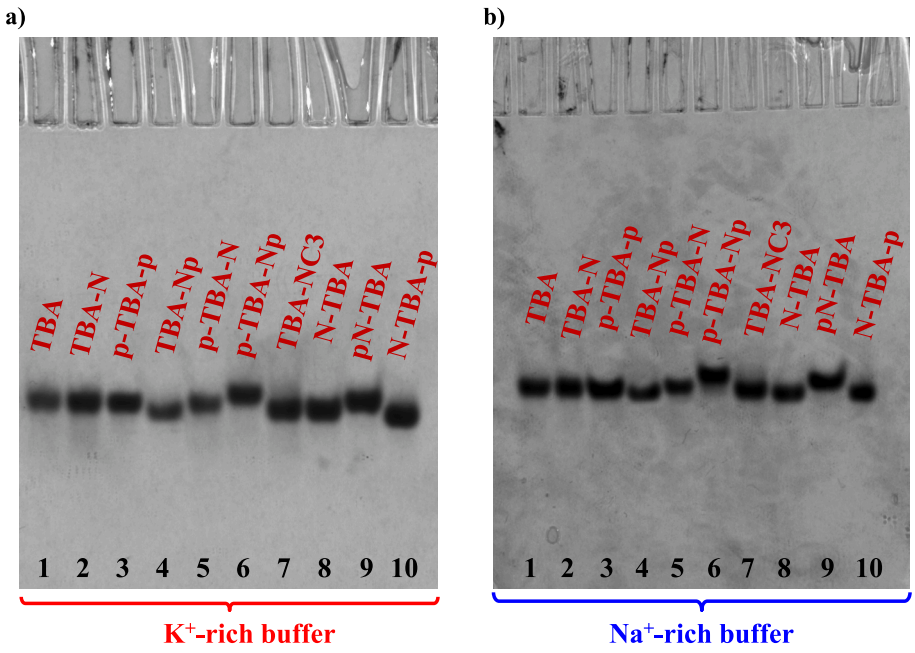

Fig. 4. Representative 15 % polyacrylamide gel electrophoresis under native conditions of the oligonucleotide samples at 15 μM concentration in the selected K^+- (**a**) and Na^+-rich (**b**) buffer solutions, run at 80 V at r.t. for 1.45 h in TBE 1X buffer; lane 1: **TBA**; lane 2: **TBA-N**; lane 3: **p-TBA-p**; lane 4: **TBA-Np**; lane 5: **p-TBA-N**; lane 6: **p-TBA-Np**; lane 7: **TBA-NC3**; lane 8: ***N*-TBA**; lane 9: **pN-TBA**; lane 10: ***N*-TBA-p**.

resistance under the explored conditions. Finally, the least stable derivatives proved to be **N-TBA** and **pN-TBA**. These compounds were completely degraded after 3 and 2 h FBS incubation, respectively, showing $t_{1/2}$ values even lower than unmodified TBA.

Therefore, the general trend of serum nuclease resistance is: **TBA-Np** > **TBA-N** > **N-TBA-p** > **TBA-NC3** > **p-TBA-Np** > **p-TBA-N** > **p-TBA-p** > TBA > **N-TBA** > **pN-TBA** (Figs. 5 and S33).

In general, these results evidenced that the insertion of the NDI group at the 3′-end (**TBA-N**) led to a marked enhancement of the nuclease stability with respect to unmodified TBA ($t_{1/2}$ of 6.0 vs. 0.6 h), which was sensibly reduced when the HPP group was added at the 5′-end or at both extremities (**p-TBA-N** and **p-TBA-Np**), providing derivatives with lower $t_{1/2}$ values (1.9 and 2.1 h, respectively) than **TBA-N**. However, both derivatives showed improved nuclease resistance compared to unmodified TBA. In turn, if HPP was added at the 3′-end, as in the case of **TBA-Np**, no significant differences in the nuclease stability were observed ($t_{1/2}$ value of 6.3 h), whereas the removal of the hydroxyl in **TBA-NC3** led to a lower resistance to degradation ($t_{1/2}$ value of 4.9 h).

Notably, the introduction of the NDI moiety at the 5′-end alone (**N-TBA**) or in association with the HPP group (**pN-TBA**) led to a faster degradation with respect to TBA itself, with $t_{1/2}$ values respectively of ca. 0.5 and 0.3 h. In contrast, the addition of one HPP group at the 3′-end of *N*-TBA (**N-TBA-p**) led to a marked increase of the nuclease stability of the oligonucleotide ($t_{1/2}$ = 5.8 h). These data comprehensively demonstrated that the resistance to enzymatic degradation of the TBA analogues with respect to unmodified TBA was not only correlated to the specific nature of the inserted probe but also to its position. Indeed, a higher resistance to serum degradation was observed for the 3′-conjugated oligonucleotides than for the 5′-conjugated derivatives, in line with the general observation that the degradation in serum is mainly driven by 3′-exonuclease activity.[69] Overall, a 5′,3′-bis-conjugation did not guarantee *per se* higher resistance to nucleases, this being anyway correlated with the stability and compactness of the G-quadruplex structure of the aptamer.

2.2.5. *Coagulation experiments*

All the TBA analogues were then evaluated for their ability to inhibit the fibrinogen hydrolysis in comparison with their natural counterpart by a thrombin clotting time assay. In detail, the thrombin-induced clotting of fibrinogen was measured spectrophotometrically, following over time the increase in absorbance at 380 nm caused by fibrin formation. If aptamers bind to the protein, the time required to induce clot formation is prolonged to an extent depending on their potency as inhibitors of the thrombin activity.

Normalized UV intensity curves as a function of time at 1:5 thrombin: aptamer molar ratio and in the absence of oligonucleotides were reported in Fig. 6a, while clotting times were depicted in Fig. 6b.

Aiming at quantitatively comparing the thrombin inhibition ability observed for unmodified TBA and its modified derivatives, the anticoagulant activity of each oligonucleotide was determined also as previously performed[16–18] in terms of ratio between the coagulation rate determined in the presence of the tested aptamer and in the absence of any inhibitor, and reported in Table S5 as mean values ± SE.

Inspection of Fig. 6a revealed that, in the absence of aptamers, a quick and steep increment of absorbance intensity was found, suggesting a rapid thrombin-catalyzed fibrin formation. In contrast, upon addition of the investigated aptamers, a long lag time associated with a more slowly scattered intensity increase was observed, evidencing a net inhibition of thrombin coagulation activity (Fig. 6a).

Although all the tested compounds were able to affect the protein activity on fibrinogen (Fig. 6 and Table S5), our results evidenced marked differences among the TBA analogues in their ability to inhibit the clotting formation.

In detail, **TBA-N** and **p-TBA-N** exhibited an anticoagulant activity slightly improved compared to unmodified TBA, with clotting time values of ca. 30 vs. 22 *sec* of their parent aptamer. In contrast, **p-TBA-p**, **TBA-Np**, **TBA-NC3**, **N-TBA** and **pN-TBA** showed a markedly improved ability to retard fibrin formation, with anticoagulant activity respectively of 5.2-, 5.0-, 3.5-, 6.9- and 7.0-fold higher than the native aptamer. The most active compounds in this series were **p-TBA-Np** and **N-TBA-p**, with significant thrombin inhibitory activity, respectively increased 9.7- and 11.1-fold with respect to their natural counterpart (Table S5).

The general trend of anticoagulant activity obtained is: **N-TBA-p** > **p-TBA-Np** > **pN-TBA** ≈ **N-TBA** > **p-TBA-p** ≈ **TBA-Np** > **TBA-NC3** > **p-TBA-N** ≈ **TBA-N** > TBA. The presence of the NDI conjugating group was

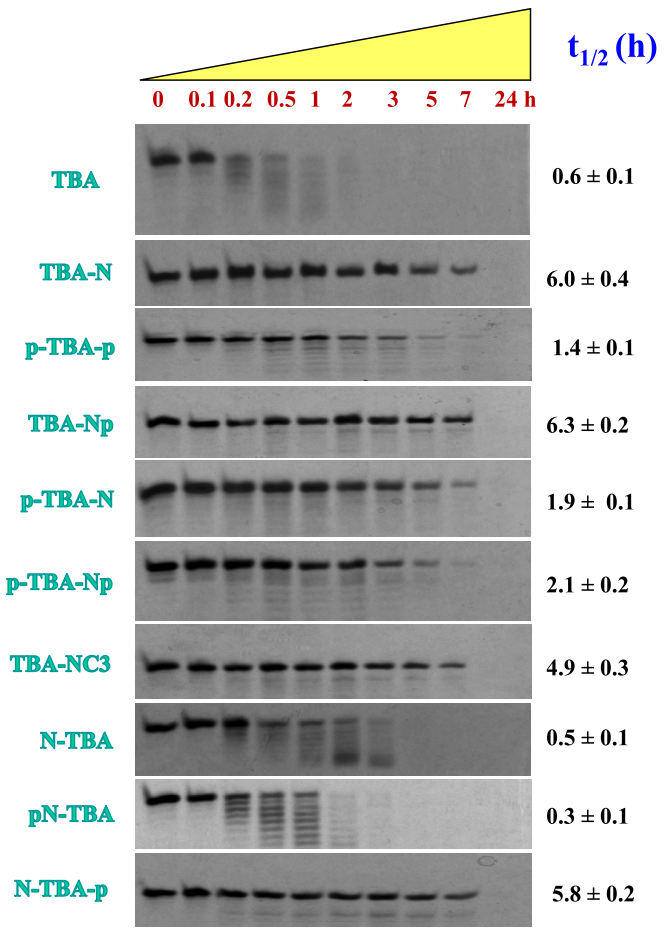

Fig. 5. Enzymatic resistance experiments performed after incubating the oligonucleotides in 80 % FBS, as monitored by 20 % denaturing polyacrylamide gel electrophoresis up to 24 h (time points: 0, 0.1, 0.2, 0.5, 1, 2, 3, 5, 7 and 24 h). For each compound, a representative 20 % denaturing PAGE (8 M urea) was reported: samples were loaded at 15 μM concentration and the gels were run at constant 200 V at r.t. for 2.5 h in TBE 1X as running buffer.

in general always effective in improving the anticoagulant activity of the native aptamer (Fig. 6 and Table S5). Interestingly, the presence of the HPP group at both TBA extremities proved to be beneficial (cfr. **p-TBA-p** vs. **TBA** and **p-TBA-Np** vs. **TBA-N**), as previously found for the pseudo-cyclic TBA series.[18] Noteworthy, the introduction of a single HPP moiety at the 3′-end also enhanced the inhibitory activity, as observed comparing **TBA-Np** vs. **TBA-N** and **N-TBA-p** vs. **N-TBA** (Fig. 6 and Table S5). The absence of the terminal hydroxyl function in **TBA-NC3** induced a slight decrease of the inhibitory activity. On the contrary, the presence of a single HPP group at the 5′-end of the TBA sequence did not affect the anticoagulant activity of its parent compound (cfr. **pN-TBA** vs. ***N*-TBA** and **p-TBA-N** vs. **TBA-N**, Fig. 6 and Table S5).

Furthermore, to verify if **p-TBA-Np** and **N-TBA-p** were more or less efficient as thrombin inhibitors than the previously studied cyclic and pseudo-cyclic derivatives, **cycTBA II** from the cyclic series[17] along with **TBA-NNp/DDp** and **TBA-Np/Np** from the pseudo-cyclic one[18] – chosen for being the most active oligonucleotides from our previous studies – were studied in parallel under the same experimental conditions here tested (Fig. 7 and Table S5).

As previously estimated through light scattering measurements, [17,18] **cycTBA II** proved to be more active than **TBA-NNp/DDp** which in turn was a more potent inhibitor than **TBA-Np/Np** (Fig. 7 and Table S5). Remarkably, under the same explored conditions, both **p-TBA-Np** and **N-TBA-p** inhibited clot formation more efficiently than the best TBA analogues previously developed by our groups (Fig. 7 and Table S5).

Finally, both **p-TBA-Np** and **N-TBA-p** were also tested at higher concentrations, i.e. at 1:10 thrombin:aptamer molar ratio (Fig. S34 and Table S5). Both aptamers exhibited sensibly prolonged clotting times at higher doses (Fig. S34), thus confirming a dose–response behavior and denoting a superior anticoagulant activity of ca. 22 and 26 times, respectively, vs. native TBA (Table S5).

3. Conclusions

Since its first identification in 1992,[70] TBA has always aroused strong interest in both therapy and diagnostics of coagulation diseases as well as in surgery, being also elected as a good model for proof-of-concept studies. Thus it is not surprising that, being an aptamer with a well-defined G-quadruplex structure, in the last 30 years a large number of punctual or more extensive modifications have been proposed in order to obtain definitive structure–activity relationships and, mainly, more active aptamers for in vivo applications.[15] From the large body of data acquired on the variety of diverse TBA analogues described in the literature clearly emerges that, even if some general rules are valid, each modification has to be evaluated individually and the specific effects, which are generally position-dependent, are not always predictable.[15]

Considering the urgent need for efficient antithrombotic agents capable of inhibiting the fibrinogen-fibrin conversion promoted by thrombin under pathological conditions, chemical modifications of the TBA structure are still actively and widely explored. Research efforts in this field have been devoted much more frequently to modify the oligonucleotide backbone of TBA, with modifications at the level of the nucleobases, sugars or phosphodiester bonds, and more rarely to insert proper derivatizations at the TBA extremities.[66,68,71,72] In principle, terminal modifications are much easier introduced and ensure an enhanced resistance to enzymatic degradation operated by nucleases, as well-demonstrated for some already known TBA analogues.[66,68] In addition, this approach allows maintaining the main core of the aptamer and thus the capability to recognize the thrombin binding site, i.e. exosite I.[15]

Starting from this scenario and also taking into account our previous studies,[18] in this work we have explored a new design of TBA derivatives, carrying NDI appendages at the 3′- or 5′-end accompanied or not by HPP groups. Indeed, the conjugation of TBA with an NDI moiety proved to improve both G-quadruplex thermal stability and nuclease resistance, while the presence of HPP groups at TBA extremities generally provided derivatives with lower G-quadruplex thermal stability but higher resistance to nuclease degradation in serum and enhanced ability to inhibit thrombin compared to the parent aptamer. [18]

The analysis of G-quadruplex thermal stability data of this new set of TBA derivatives – performed by both UV and CD measurements – showed that the insertion of two HPP groups at both TBA extremities was detrimental for the thermal stability of the G4 structure compared to the parent aptamer. In turn, the presence of a single HPP group produced different effects depending on its specific position: in general, its insertion at the 5′-end led to a marked destabilization, whereas its addition at the 3′ extremity had no dramatic effects or led only to a slight destabilization of the G-quadruplex core of TBA. In contrast, the presence of the NDI moiety in all cases significantly improved the thermal stability of the unmodified TBA, no matter if it was inserted at the 5′ or 3′ end.

The resistance to enzymatic degradation of the TBA analogues compared to their parent aptamer was indeed correlated to the specific nature of the inserted probe but mainly influenced by its position. A higher resistance to serum degradation was observed for the 3′-conjugated oligonucleotides than for the 5′-modified derivatives, while the 5′,3′-bis-conjugation with HPP groups had detrimental effects on the aptamer enzymatic stability.

The evaluation of the anticoagulant activity confirmed the beneficial effect of the HPP group at both TBA extremities, as previously found for

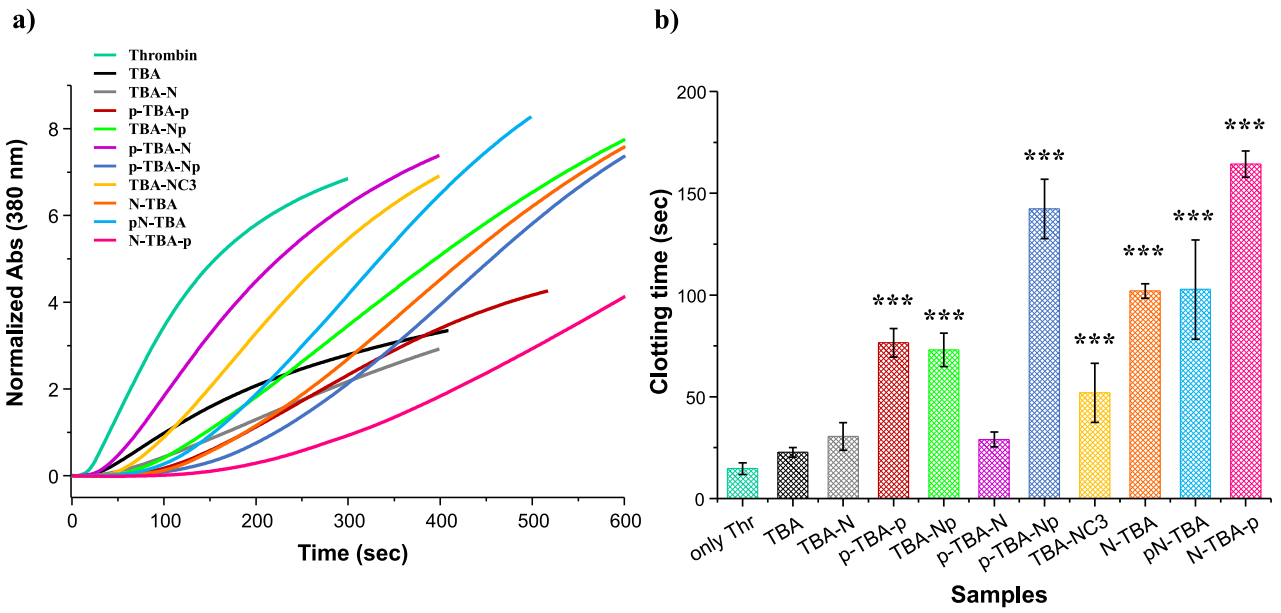

Fig. 6. **a**) Representative normalized coagulation curves for the TBA analogues and unmodified TBA at 1:5 thrombin:aptamer molar ratio in PBS, as determined spectrophotometrically following the thrombin-catalyzed conversion of fibrinogen into fibrin (fibrinogen: 1.8 mg/mL, α-thrombin: 5 nM). A representative curve in the absence of aptamers (Thr) is also reported for comparison. **b**) Fibrinogen clotting times (*sec*) as determined from the maxima of the second derivative of each obtained scattering curve. Data are reported as mean values ± SE (error bars) for multiple determinations. Statistical significance was assessed by using Student's *t*-test: *p < 0.1, **p < 0.05 or ***p < 0.01 vs. unmodified TBA.

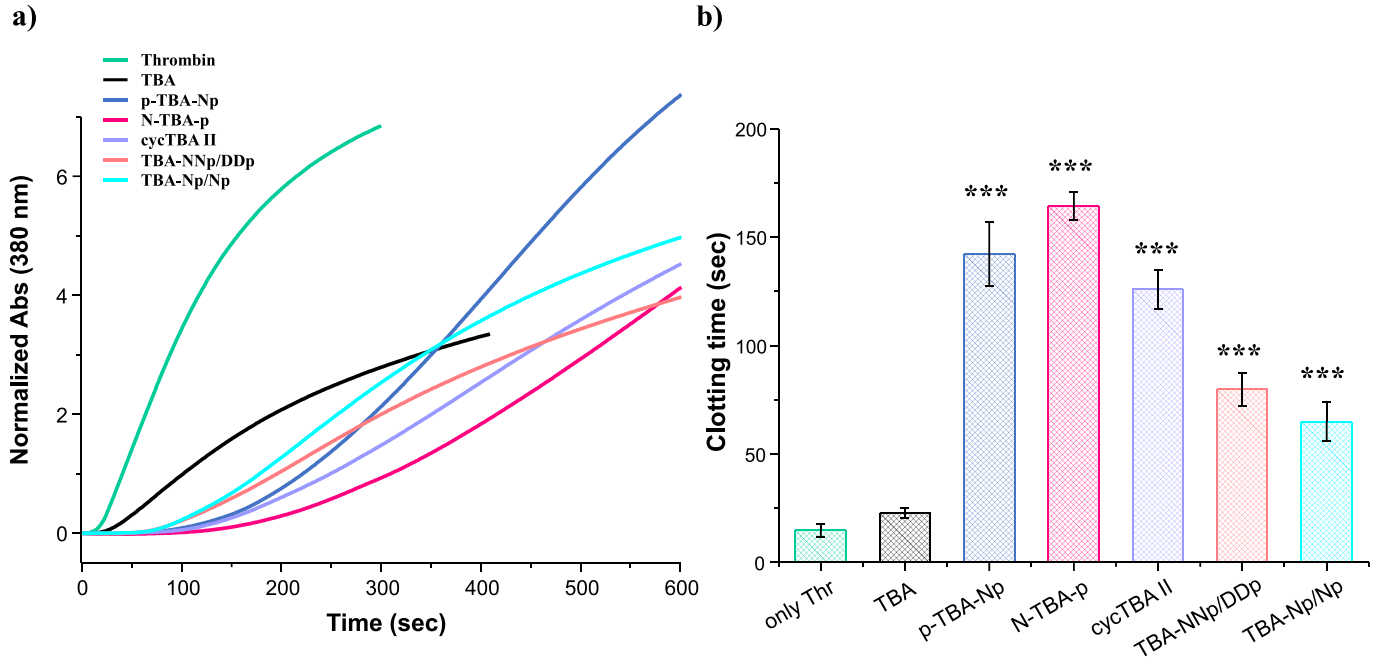

Fig. 7. **a**) Representative normalized coagulation curves for the most active TBA analogues of this series, unmodified TBA and previously studied **cycTBA II**, **TBA-NNp/DDp** and **TBA-Np/Np** at 1:5 thrombin:aptamer molar ratio in PBS, as determined spectrophotometrically following the thrombin-catalyzed conversion of fibrinogen into fibrin (fibrinogen: 1.8 mg/mL, α-thrombin: 5 nM). A representative curve in the absence of aptamers (Thr) is also reported for comparison. **b**) Fibrinogen clotting times (*sec*) as determined from the maxima of the second derivative of each obtained scattering curve. Data are reported as mean values ± SE (error bars) for multiple determinations. Statistical significance was assessed by using Student's *t*-test: *p < 0.1, **p < 0.05 or ***p < 0.01 vs. unmodified TBA.

the pseudo-cyclic TBA series.[18] Noteworthy, the introduction of a single HPP moiety at the 3′-end also enhanced the aptamer inhibitory activity, while the same conjugation at the 5′ extremity of the TBA sequence did not produce significant effects. Regarding the NDI probe, its insertion was always beneficial for the TBA antithrombin activity.

Considering the mono-conjugated analogues altogether, our results showed that 3′-modifications are indeed better than 5′-ones both in terms of nuclease resistance and anticoagulant activity and thus are somehow to be preferred. This is in line with the results reported by Uehara and coworkers, who evaluated the attachment of a 20-unit poly (dA) tail to the 3′-end of TBA. This conjugation proved to reduce the enzymatic degradation in human plasma and enhance the clotting inhibitory activity with respect to the native TBA.[66]

Noteworthy is the comparison between **p-TBA-N** and **N-TBA-p**,

which, although having the same appendages at inverted extremity, were featured by very different properties, thus highlighting the importance not only of the specific probe inserted but also of its position on the TBA sequence. Indeed, while **N-TBA-p** proved to be very resistant in serum and very effective as thrombin inhibitor, **p-TBA-N** was one of the worst analogues investigated, both in terms of nuclease resistance ($t_{1/2}$ of 1.9 h) and thrombin inhibition (anticoagulant activity of 2, i.e. only 2-fold increase compared to the system in the absence of aptamer).

Considering all the different aspects involved in potential applications in vivo of anticoagulant aptamers, the whole set of data indicated **N-TBA-p** as a very promising candidate for future more in-depth studies, showing clotting times superior to the best cyclic and pseudo-cyclic TBA derivatives previously investigated. In addition, this aptamer is also featured by an enhanced G-quadruplex thermal stability (ΔT_m of + 14 in both the selected K^+-rich and Na^+-rich solutions) and ca. 9.7-fold improved nuclease resistance. Taken together, this study shows that also minimal, point modifications, also very easily introduced in oligonucleotide backbones, can dramatically enhance the properties of aptamers, and this further confirms the enormous and still limitedly explored potential of this class of biomolecules in both therapy and diagnostics.

4. Materials and methods

General methods. All the reagents and solvents were of the highest commercially available quality and were used as such. Nuclease-free water, acrylamide/bis-acrylamide (19:1) 40 % solution, Tris-Borate-EDTA (TBE) 10X, glycerol, formamide and urea were purchased from VWR. Stains-All, ammonium persulfate (APS) and tetramethylethylenediamine (TEMED) were purchased from Sigma Aldrich (Merck Life Science S.r.l.). Fetal Bovine Serum (FBS) was provided by Euroclone.

Unmodified TBA was purchased as HPLC-purified oligonucleotide from biomers.net GmbH (Germany), which provided MALDI-TOF mass spectrometry and HPLC data fully confirming its identity and purity. In turn, all the TBA analogues of this series were synthesized and purified as described below. The purity of all the oligonucleotides was further validated, just prior use, by 20 % PAGE analysis under denaturing conditions (see Fig. S1).

Oligonucleotide synthesis. The solid-supported synthesis of modified TBA derivatives was performed on a 394 ABI DNA synthesizer. All the conventional reagents, solvents for DNA synthesis, N^2-*tert*-butylphenoxyacetyl-deoxyguanosine and thymidine phosphoramidites were purchased from ChemGenes© Corporation and Biosolve© Chimie. The oligonucleotides were elongated from corresponding solid supports on the DNA synthesizer, with a 1 μmol scale cycle, according to standard phosphoramidite chemistry protocols. The detritylation step was performed for 65 s using a 3 % TCA solution in CH_2Cl_2. For the coupling step, benzylmercaptotetrazole (0.3 M in anhydrous CH_3CN) was used as the activator agent with modified **2**, **3** or **6** phosphoramidites (0.1 M in CH_3CN, 3 min coupling time) and standard nucleoside phosphoramidites (0.1 M in CH_3CN, 90 s coupling time). The capping step was performed with phenoxyacetic anhydride using commercially available solutions (Cap A: phenoxyacetic anhydride:pyridine:THF 10:10:80 v/v/v; Cap B: 10 % *N*-methylimidazole in THF) for 20 s. The oxidation step was performed with a standard, diluted iodine solution (0.1 M I_2, THF: pyridine:water 90:5:5, v/v/v) for 15 s. Oligonucleotides were deprotected and released from the CPG support by treatment with a 7 N solution of NH_3/MeOH for 4–6 h at 55 °C on a thermoshaker. Standard deprotection treatment with concentrated aqueous ammonia was here avoided since it proved to lead to partial degradation of the NDI moieties. After deprotection, the CPG beads were then washed with anhydrous MeOH. The eluate and the washing were pooled and dried on a speed vacuum. Then the CPG beads were further washed with water, the eluate was pooled with the previous fractions and dried under vacuum.

All the oligonucleotides were analyzed and purified by RP-HPLC and then characterized by MALDI-TOF mass spectrometry. RP C18 HPLC spectra were acquired using a linear gradient from 1 % to 40 % of CH_3CN in 50 mM TEAAc buffer (pH = 7) over 20 min. The C18 RP-HPLC and MALDI-TOF MS analysis of the TBA analogues are reported in the supporting information (Figs. S35-S42). For TBA-N see Pérez de Carvasal, K. *et al.*[18]

Preparation of the oligonucleotide samples. Purified and lyophilized oligonucleotides were dissolved in a proper amount of nuclease-free water. Their concentration was determined by UV analysis recording the absorbance at 260 nm and 95 °C. A JASCO V-770 UV–vis spectrophotometer equipped with a Peltier Thermostat JASCO ETCS-761 and a quartz cuvette with a 1 cm path length (1 mL internal volume, Hellma) were used for all the measurements. For all the oligonucleotides, the molar extinction coefficient of 158.480 cm^{-1} M^{-1} – calculated for the unstacked oligonucleotides using the Oligo Calculator online program[73] – was used to determine the exact concentration of the prepared stock solutions. The absorbance spectra were recorded in the 220–320 nm range setting a medium response, a scanning speed of 100 nm/min and a 2.0 nm bandwidth with the appropriate baseline subtracted. Taking a suitable aliquot from the initial stock solutions in H_2O, all the investigated oligonucleotides were then diluted in the selected K^+- (10 mM KH_2PO_4/K_2HPO_4, 70 mM KCl, 0.2 mM EDTA, pH = 7.2) or Na^+-rich (PBS: 137 mM NaCl, 2.7 mM KCl, 10 mM NaH_2PO_4/Na_2HPO_4, 1.8 mM KH_2PO_4/K_2HPO_4, pH = 7.3) phosphate buffer solutions. Then, for each experiment, the samples were treated by heating them for 5 min at 95 °C and thereafter left to slowly cool to r.t. overnight, so to favor their structuring into the thermodynamically most stable G-quadruplex conformations.[74] The annealed samples were finally stored at 4 °C until use.

UV spectroscopy. All the UV measurements were performed on a JASCO V-770 UV–vis spectrophotometer equipped with a Peltier Thermostat JASCO ETCS-761, by using a quartz cuvette with a 1 cm path length (1 mL internal volume, Hellma).

UV–vis spectra. Absorbance spectra at r.t. were recorded using a 2 μM solution of the investigated oligonucleotides, prepared in HPLC grade water after proper dilution of their stock solutions. UV–vis spectra (2 accumulations) were recorded in the 220–800 nm range with a scanning speed of 100 nm/min and a 2.0 nm bandwidth with the proper baseline subtracted. Each experiment was performed in duplicate.

UV Thermal Difference Spectra. UV spectra for thermal difference spectra (TDS) analysis were recorded at 2 μM oligonucleotide concentration in the selected phosphate buffer solutions. In detail, the absorbance spectra (2 accumulations) were recorded at 15 and 90 °C in the 220–320 nm range using a scanning speed of 100 nm/min with the proper baseline subtraction.[31,35] Then, TDS data derived by the subtraction of the UV spectrum recorded at 90 °C (i.e. a temperature far above the T_m), where the G-quadruplex structure is unfolded, from the one obtained at 15 °C (i.e. a temperature well below the T_m), at which the oligonucleotide is fully folded.[34,35,37] To better compare the spectral data, TDS were then normalized dividing all the raw data in the 220–320 range by its highest value.[34] From normalized spectra, three TDS factors ($\Delta A_{240}/\Delta A_{295}$, $\Delta A_{255}/\Delta A_{295}$ and $\Delta A_{275}/\Delta A_{295}$) were also determined as the ratios between the absolute absorbance values at the selected wavelengths.[34,36]

UV thermal denaturation/renaturation experiments. Absorbance vs. temperature profiles of all the oligonucleotides were monitored following the absorbance changes at 295 nm in the 15–90 °C temperature range using a scan rate of 1 °C/min.[35,38] UV-monitored thermal denaturation/renaturation curves were reported as normalized ΔA values (NΔA) as a function of the temperature, converting UV data as previously described.[75] Apparent T_m values were determined as the minimum and the maximum of the first derivative plots of the heating and cooling profiles, respectively, and the error associated with the T_m determination was ± 1 °C. Each experiment was performed in duplicate.

Circular dichroism (CD) spectroscopy. CD spectra and CD-monitored thermal denaturation/renaturation curves were recorded on a Jasco J-1500 spectropolarimeter equipped with CTU-100

circulating thermostat unit, by using a quartz cuvette with a 1 cm path length (3 mL internal volume, Hellma). All the spectra were recorded using the following parameters: spectral window 220–320 nm, data pitch 1 nm, bandwidth 2 nm, response 4 s, scanning speed 100 nm/min, 3 accumulations, and were then corrected by subtracting the proper blank.[42] For CD studies, all the oligonucleotides were analyzed at 2 μM concentration in both saline conditions.

For both the K^+- and Na^+-rich buffer solutions, heating/cooling curves were recorded in the 15–90 °C temperature range following the CD signal at 295 nm vs. the temperature, using a scan rate of 1 °C/min and recording the CD spectra from 220 to 320 nm in 5 °C steps. Each experiment was performed in triplicate.

For both CD spectra and CD melting/cooling profiles, the unit of the Y axis was converted from millidegrees to the molar ellipticity [θ] (deg cm^2 $dmol^{-1}$) using the equation $[\theta] = \theta/10 \times l \times C$, where θ is the observed CD ellipticity in millidegrees, C is the oligonucleotide concentration in mol/L, and l is the optical path length of the cell expressed in cm. To better compare CD profiles of different oligonucleotides, data from heating/cooling curves were also converted into folded fraction (α) using the equation $\alpha = [\theta_{obs}(T) - \theta_U)/(\theta_F - \theta_U)]$, where $\theta_{obs}(T)$ is the molar ellipticity observed for each temperature, while θ_F and θ_U are the molar ellipticity values found for the structured (T = 15 °C) and fully denatured (T = 90 °C) oligonucleotide, respectively.

The T_m values were estimated as the minima and maxima of the first derivative plots of the melting and cooling curves, respectively, with an associated error of ± 1 °C. ΔT_m, values were determined by subtracting the T_m of unmodified TBA from that calculated for each TBA analogue.

The CD-melting profiles exhibited in all cases a sigmoidal behavior and were thus analyzed by using the van't Hoff equation to determine the thermodynamic parameters associated with the G-quadruplex unfolding, as previously performed.[18,75] In detail, ΔH^0 and ΔS^0 values were directly calculated from the experimental CD data using the Marquardt non-linear least-squares method used by Petersheim and Turner[76] adapted to a monomolecular system,[53] under the assumption that ΔCp is equal to zero. All the thermodynamic parameters are expressed in kJ/mol as mean values ± SD, as determined from multiple determinations. ΔG^0 values were then calculated at 298 K from the equation $\Delta G^0 = \Delta H^0 - T\,\Delta S^0$.

5. Polyacrylamide gel electrophoresis (PAGE) analysis

Denaturing PAGE. PAGE experiments under denaturing conditions were carried out following previously described protocols,[77] with minor modifications. Briefly, 3 μL of a 35 μM solution of each oligonucleotide in water were mixed with formamide (1:2, v/v) to completely unfold the samples, heated at 95 °C for 5 min, then left in contact with ice until gel loading. Thereafter, all these mixtures – supplemented with 5 % glycerol – were loaded on 20 % denaturing gels (8 M urea). The gels were run at r.t. at constant 200 V for 2.5 h using TBE 1X as running buffer. Then, gels were stained overnight with a Stains-All solution prepared according to the manufacturer's instructions and finally visualized with a UV transilluminator (BioRad ChemiDoc XRS). Each experiment was performed in triplicate.

Native PAGE. All the oligonucleotides were dissolved at 15 μM concentration in both the selected K^+- and Na^+-rich buffer solutions and then slowly annealed as previously described. Then, these samples – supplemented with 5 % glycerol – were loaded on 15 % polyacrylamide gels, which were run, under native conditions, at 80 V at r.t. for 1.45 h using TBE 1X as running buffer.

Gels were then stained overnight with a Stains-All solution prepared according to the manufacturer's instructions and finally visualized with a UV transilluminator (BioRad ChemiDoc XRS). Each experiment was performed at least in triplicate.

Enzymatic stability assays monitored by gel electrophoresis analysis. The evaluation of the oligonucleotide resistance in serum was carried out by gel electrophoresis analysis according to previous procedures,[78,79] with minor modifications. Briefly, all the oligonucleotides were first slowly annealed in PBS at 250 μM conc., then incubated in 80 % v/v FBS at 37 °C. At fixed times, 3 μL (150 pmols) of each sample from these oligo/FBS mixtures were collected, mixed with formamide (1:2, v/v) to immediately stop the nuclease action, heated at 95 °C for 5 min, and finally stored at −20 °C until their use. Thereafter, all the samples – complemented with 5 % glycerol just before loading – were analyzed by electrophoresis on 20 % PAGE using 8 M urea in TBE 1X as running buffer. All the gels were run at r.t. at constant 200 V for 2.5 h, then stained overnight with a Stains-All solution prepared according to the manufacturer's instructions and finally visualized with a UV transilluminator (BioRad ChemiDoc XRS). Each experiment was performed at least in triplicate. The intensity of DNA bands on the gel, at each collected time, was then quantified using the FiJi software and normalized with respect to the oligonucleotides not treated with FBS. Percentages of the remaining intact oligonucleotide are determined and expressed as mean values ± SD for multiple determinations. Half-life times ($t_{1/2}$) of each oligonucleotide were then derived by fitting the percentage values at each collected time with an equation for first order kinetics.

Fibrinogen clotting times. The thrombin-induced clotting of fibrinogen was measured spectrophotometrically, on a JASCO V-770 UV–vis spectrophotometer, following previously described protocols.[80,81] Human α-thrombin and fibrinogen from human plasma were purchased from Haematologic Technologies and Sigma-Aldrich, respectively. For these assays, oligonucleotides were suspended in the selected Na^+-rich buffer, i.e. PBS, at a concentration of 10 μM and then slowly annealed. Then, oligonucleotides (1:5 or 1.10 M ratio to thrombin, as specified) were incubated for 2 min in 1 mL of PBS containing 1.8 mg/mL of fibrinogen in a PMMA cuvette (volume 1.5 mL, cell length 1 cm, Brand). Finally, α-thrombin was added up to a final concentration of 5 nM. The time required for fibrin polymerization was determined from UV scattering curves recording at r.t. the absorbance (wavelength fixed at 380 nm) in the presence of each oligonucleotide (data interval: 1 s). The blank clotting curve was determined by measuring the absorbance in the absence of any inhibitor. Each experiment was repeated at least in triplicate. Normalized coagulation curves were obtained by converting the absorbance data using the equation nAbs = [Abs (t) - Abs (0)] / Abs (0), where Abs (t) and Abs (0) are the absorbance values at time t and at the beginning of the experiment. Clotting time values were derived from the maximum of the second derivative of each scattering curve and reported as mean values ± SE for multiple determinations. Anticoagulant activity was calculated as the ratio between the coagulation rate in the presence of each oligonucleotide and in the presence of thrombin alone and was reported as mean values ± SE for multiple determinations.

The statistical significance of replicates was analyzed using Student's *t*-test with $^*p < 0.1$, $^{**}p < 0.05$ or $^{***}p < 0.01$.

Funding: The research leading to these results has received funding from AIRC (Associazione Italiana per la Ricerca sul Cancro) under IG 2020-ID. 25046-P.I. Montesarchio Daniela.

Declaration of Competing Interest

The authors declare that they have no known competing financial interests or personal relationships that could have appeared to influence the work reported in this paper.

Acknowledgements

K.P.d.C. thanks the University of Montpellier for the award of a research studentship. F.M. is member of INSERM. The authors thank Ilaria Caliendo, hosted in D.M. laboratories within her Master thesis in Chemistry, for her precious help in data acquisition and curation.

Appendix A. Supplementary data

Supplementary data to this article can be found online at https://doi.org/10.1016/j.bioorg.2023.106917.

References

[1] A. Aviñó, C. Fàbrega, M. Tintoré, R. Eritja, Thrombin binding aptamer, more than a simple aptamer: chemically modified derivatives and biomedical applications, Curr. Pharm. Des. 18 (2012) 2036–2047, https://doi.org/10.2174/138161212799958387.

[2] D. Musumeci, D. Montesarchio, Polyvalent nucleic acid aptamers and modulation of their activity: a focus on the thrombin binding aptamer, Pharmacol. Ther. 136 (2012) 202–215, https://doi.org/10.1016/j.pharmthera.2012.07.011.

[3] B. Deng, Y. Lin, C. Wang, F. Li, Z. Wang, H. Zhang, X.F. Li, X.C. Le, Aptamer binding assays for proteins: the thrombin example-a review, Anal. Chim. Acta 837 (2014) 1–15, https://doi.org/10.1016/j.aca.2014.04.055.

[4] E.G. Zavyalova, N. Ustinov, A. Golovin, G. Pavlova, A. Kopylov, G-quadruplex aptamers to human thrombin versus other direct thrombin inhibitors: the focus on mechanism of action and drug efficiency as anticoagulants, Curr. Med. Chem. 23 (2016) 2230–2244, https://doi.org/10.2174/0929867323666161031612508.

[5] D. Musumeci, C. Platella, C. Riccardi, F. Moccia, D. Montesarchio, Fluorescence sensing using DNA aptamers in cancer research and clinical diagnostics, Cancers 9 (2017) 174–217, https://doi.org/10.3390/cancers9120174.

[6] C. Riccardi, E. Napolitano, D. Musumeci, D. Montesarchio, Dimeric and multimeric DNA aptamers for highly effective protein recognition, Molecules 25 (2020) 5227, https://doi.org/10.3390/molecules25225227.

[7] E. Di Cera, Thrombin, Mol. Aspects Med. 29 (2008) 203–254, https://doi.org/10.1016/j.mam.2008.01.001.

[8] L.G. Licari, J.P. Kovacic, Thrombin physiology and pathophysiology, J. Vet. Emerg. Crit. Care 19 (2009) 11–22, https://doi.org/10.1111/j.1476-4431.2009.00383.x.

[9] I. Russo Krauss, A. Merlino, C. Giancola, A. Randazzo, L. Mazzarella, F. Sica, Thrombin-aptamer recognition: a revealed ambiguity, Nucleic Acids Res. 39 (2011) 7858–7867, https://doi.org/10.1093/nar/gkr522.

[10] I. Russo Krauss, A. Merlino, A. Randazzo, E. Novellino, L. Mazzarella, F. Sica, High-resolution structures of two complexes between thrombin and thrombin-binding aptamer shed light on the role of cations in the aptamer inhibitory activity, Nucleic Acids Res. 40 (2012) 8119–8128, https://doi.org/10.1093/nar/gks512.

[11] A. Pica, I. Russo Krauss, A. Merlino, S. Nagatoishi, N. Sugimoto, F. Sica, Dissecting the contribution of thrombin exosite I in the recognition of thrombin binding aptamer, FEBS J. 280 (2013) 6581–6588, https://doi.org/10.1111/febs.12561.

[12] S.M. Nimjee, C.P. Rusconi, R.A. Harrington, B.A. Sullenger, The potential of aptamers as anticoagulants, Trends Cardiovasc. Med. 15 (2005) 41–45, https://doi.org/10.1016/j.tcm.2005.01.002.

[13] A. Schwienhorst, Direct thrombin inhibitors - a survey of recent developments, Cell. Mol. Life Sci. 63 (2006) 2773–2791, https://doi.org/10.1007/s00018-006-6219-z.

[14] G. Mayer, F. Rohrbach, B. Pötzsch, J. Müller, Aptamer-based modulation of blood coagulation, Hamostaseologie 31 (2011) 258–263, https://doi.org/10.5482/ha-1156.

[15] C. Riccardi, E. Napolitano, C. Platella, D. Musumeci, D. Montesarchio, G-quadruplex-based aptamers targeting human thrombin: discovery, chemical modifications and antithrombotic effects, Pharmacol. Ther. 217 (2021), 107649, https://doi.org/10.1016/j.pharmthera.2020.107649.

[16] C. Riccardi, A. Meyer, J.J. Vasseur, I. Russo Krauss, L. Paduano, R. Oliva, L. Petraccone, F. Morvan, D. Montesarchio, Stability is not everything: the case of the cyclization of the thrombin binding aptamer, Chembiochem 20 (2019) 1789–1794, https://doi.org/10.1002/cbic.201900045.

[17] C. Riccardi, A. Meyer, J.J. Vasseur, I. Russo Krauss, L. Paduano, F. Morvan, D. Montesarchio, Fine-tuning the properties of the thrombin binding aptamer through cyclization: effect of the 5′-3′ connecting linker on the aptamer stability and anticoagulant activity, Bioorg. Chem. 94 (2020), 103379, https://doi.org/10.1016/j.bioorg.2019.103379.

[18] K. Pérez de Carvasal, C. Riccardi, I. Russo Krauss, D. Cavasso, J.J. Vasseur, M. Smietana, F. Morvan, D. Montesarchio, Charge-transfer interactions stabilize G-quadruplex-forming thrombin binding aptamers and can improve their anticoagulant activity, Int. J. Mol. Sci. 22 (2021) 9510, https://doi.org/10.3390/ijms22179510.

[19] M.M. Islam, S. Fujii, S. Sato, T. Okauchi, S. Takenaka, A selective G-quadruplex DNA-stabilizing ligand based on a cyclic naphthalene diimide derivative, Molecules 20 (2015) 10963–10979, https://doi.org/10.3390/molecules200610963.

[20] M.M. Islam, S. Sato, S. Shinozaki, S. Takenaka, Cyclic ferrocenylnaphthalene diimide derivative as a new class of G-quadruplex DNA binding ligand, Bioorg. Med. Chem. Lett. 27 (2017) 329–335, https://doi.org/10.1016/j.bmcl.2016.11.037.

[21] Z. Lv, J. Liu, W. Bai, S. Yang, A. Chen, A simple and sensitive label-free fluorescent approach for protein detection based on a Perylene probe and aptamer, Biosens. Bioelectron. 64 (2015) 530–534, https://doi.org/10.1016/j.bios.2014.09.095.

[22] N. Busschaert, D. Maity, P.K. Samanta, N.J. English, A.D. Hamilton, Improving structural stability and anticoagulant activity of a thrombin binding aptamer by aromatic modifications, Chembiochem 23 (2022) e202100670.

[23] R. Troisi, C. Riccardi, K. Pérez de Carvasal, M. Smietana, F. Morvan, P. Del Vecchio, D. Montesarchio, F. Sica, A terminal functionalization strategy reveals unusual binding abilities of anti-thrombin anticoagulant aptamers, Mol. Ther. - Nucleic Acids. 30 (2022) 585–594, https://doi.org/10.1016/j.omtn.2022.11.007.

[24] M. Al Kobaisi, S.V. Bhosale, K. Latham, A.M. Raynor, S.V. Bhosale, Functional naphthalene diimides: synthesis, properties, and applications, Chem. Rev. 116 (2016) 11685–11796, https://doi.org/10.1021/acs.chemrev.6b00160.

[25] S.V. Bhosale, M. Al Kobaisi, R.W. Jadhav, P.P. Morajkar, L.A. Jones, S. George, Naphthalene diimides: perspectives and promise, Chem. Soc. Rev. 50 (2021) 9845, https://doi.org/10.1039/d0cs00239a.

[26] C. Platella, E. Napolitano, C. Riccardi, D. Musumeci, D. Montesarchio, Disentangling the structure-activity relationships of naphthalene diimides as anticancer G-quadruplex-targeting drugs, J. Med. Chem. 64 (2021) 3578–3603, https://doi.org/10.1021/acs.jmedchem.1c00125.

[27] K. Pérez de Carvasal, N. Aissaoui, G. Vergoten, G. Bellot, J.-J. Vasseur, M. Smietana, F. Morvan, Folding of phosphodiester-linked donor–acceptor oligomers into supramolecular nanotubes in water, Chem. Commun. 57 (2021) 4130–4133, https://doi.org/10.1039/D1CC01064F.

[28] K. Pérez de Carvasal, G. Vergoten, J.J. Vasseur, M. Smietana, F. Morvan, Supramolecular recognition of phosphodiester-based donor and acceptor oligomers forming gels in water, Biomacromolecules 24 (2023) 756–765, https://doi.org/10.1021/acs.biomac.2c01203.

[29] M. Madaoui, A. Meyer, J.J. Vasseur, F. Morvan, Thermolytic reagents to synthesize 5′- or 3′-Mono(thio)phosphate oligodeoxynucleotides or 3′-modified oligodeoxynucleotides, Eur. J. Org. Chem. 2019 (2019) 2832–2842, https://doi.org/10.1002/ejoc.201900302.

[30] E.G. Zavyalova, G. Tagiltsev, R. Reshetnikov, A. Arutyunyan, A. Kopylov, Cation coordination alters the conformation of a thrombin-binding G-quadruplex DNA aptamer that affects inhibition of thrombin, Nucleic Acid Ther. 6 (2016) 299–308, https://doi.org/10.1089/nat.2016.0606.

[31] E. Largy, J.L. Mergny, V. Gabelica, Role of alkali metal ions in G-quadruplex nucleic acid structure and stability, Met. Ions Life Sci. 16 (2016) 203–258, https://doi.org/10.1007/978-3-319-21756-7_7.

[32] E. Largy, A. Marchand, S. Amrane, V. Gabelica, J.L. Mergny, Quadruplex turncoats: cation-dependent folding and stability of quadruplex-DNA double switches, J. Am. Chem. Soc. 138 (2016) 2780–2792, https://doi.org/10.1021/jacs.5b13130.

[33] D. Bhattacharyya, G.M. Arachchilage, S. Basu, Metal cations in G-quadruplex folding and stability, Front. Chem. 4 (2016) 1–14, https://doi.org/10.3389/fchem.2016.00038.

[34] J.-L. Mergny, J. Li, L. Lacroix, S. Amrane, J.B. Chaires, Thermal difference spectra: a specific signature for nucleic acid structures, Nucleic Acids Res. 33 (2005) 1–6, https://doi.org/10.1093/nar/gni134.

[35] J.-L. Mergny, L. Lacroix, UV Melting of G-quadruplexes, Curr. Protoc. Nucleic Acid Chem. 37 (2009) 17.1.1-17.1.15. Doi: 10.1002/0471142700.nc1701s37.

[36] A.I. Karsisiotis, N.M.A. Hessari, E. Novellino, G.P. Spada, A. Randazzo, M. Webba da Silva, Topological characterization of nucleic acid G-quadruplexes by UV absorption and circular dichroism, Angew. Chem. - Int. Ed. Eng. 50 (2011) 10645–10648, https://doi.org/10.1002/anie.201105193.

[37] M. Malgowska, D. Gudanis, A. Teubert, G. Dominiak, Z. Gdaniec, How to study G-quadruplex structures, J. Biotechnol. Comput. Biol. Bionanotechnol. 93 (2012) 381–390, https://doi.org/10.5114/bta.2012.46592.

[38] J.-L. Mergny, A. Phan, L. Lacroix, Following G-quartet formation by UV-spectroscopy, FEBS Lett. 435 (1998) 74–78.

[39] P.A. Rachwal, K.R. Fox, Quadruplex melting, Methods 43 (2007) 291–301, https://doi.org/10.1016/j.ymeth.2007.05.004.

[40] C. Saintomé, S. Amrane, J.L. Mergny, P. Alberti, The exception that confirms the rule: a higher-order telomeric G-quadruplex structure more stable in sodium than in potassium, Nucleic Acids Res. 44 (2016) 2926–2935, https://doi.org/10.1093/nar/gkw003.

[41] S. Poniková, M. Antalík, T. Hianik, A circular dichroism study of the stability of guanine quadruplexes of thrombin DNA aptamers at presence of K+ and Na+ ions, Gen. Physiol. Biophys. 27 (2008) 271–277.

[42] R. Del Villar-Guerra, R.D. Gray, J.B. Chaires, Characterization of quadruplex DNA structure by circular dichroism, Curr. Protoc. Nucleic Acid Chem. 68 (2017), https://doi.org/10.1002/cpnc.23, 17.8.1-17.8.16.

[43] V. Dapić, V. Abdomerović, R. Marrington, J. Peberdy, A. Rodger, J.O. Trent, P. J. Bates, Biophysical and biological properties of quadruplex oligodeoxyribonucleotides, Nucleic Acids Res. 31 (2003) 2097–2107, https://doi.org/10.1093/nar/gkg316.

[44] S. Paramasivan, I. Rujan, P.H. Bolton, Circular dichroism of quadruplex DNAs: applications to structure, cation effects and ligand binding, Methods 43 (2007) 324–331, https://doi.org/10.1016/j.ymeth.2007.02.009.

[45] J. Kypr, I. Kejnovská, D. Renčiuk, M. Vorlíčková, Circular dichroism and conformational polymorphism of DNA, Nucleic Acids Res. 37 (2009) 1713–1725, https://doi.org/10.1093/nar/gkp026.

[46] S. Masiero, R. Trotta, S. Pieraccini, S. De Tito, R. Perone, A. Randazzo, G.P. Spada, A non-empirical chromophoric interpretation of CD spectra of DNA G-quadruplex structures, Org. Biomol. Chem. 8 (2010) 2683–2692, https://doi.org/10.1039/c003428b.

[47] M. Vorlíčková, I. Kejnovská, J. Sagi, D. Renčiuk, K. Bednářová, J. Motlová, J. Kypr, Circular dichroism and guanine quadruplexes, Methods 57 (2012) 64–75, https://doi.org/10.1016/j.ymeth.2012.03.011.

[48] A. Randazzo, G.P. Spada, M. Webba da Silva, Circular dichroism of quadruplex structures, Top. Curr. Chem. 330 (2013) 67–86, https://doi.org/10.1007/128_2012_331.

[49] R. Del Villar-Guerra, J.O. Trent, J.B. Chaires, G-quadruplex secondary structure obtained from circular dichroism spectroscopy, Angew. Chem. - Int. Ed. Eng. 57 (2018) 7171–7175, https://doi.org/10.1002/anie.201709184.

[50] M. Zaitseva, D. Kaluzhny, A. Shchyolkina, O. Borisova, I. Smirnov, G. Pozmogova, Conformation and thermostability of oligonucleotide d(GGTTGGTGTGGTTGG) containing thiophosphoryl internucleotide bonds at different positions, Biophys. Chem. 146 (2010) 1–6, https://doi.org/10.1016/j.bpc.2009.09.011.
[51] I. Russo Krauss, V. Napolitano, L. Petraccone, R. Troisi, V. Spiridonova, C. A. Mattia, F. Sica, Duplex/quadruplex oligonucleotides: role of the duplex domain in the stabilization of a new generation of highly effective anti-thrombin aptamers, Int. J. Biol. Macromol. 107 (2018) 1697–1705, https://doi.org/10.1016/j.ijbiomac.2017.10.033.
[52] E.G. Zavyalova, V.A. Legatova, R.S. Alieva, A.O. Zalevsky, V.N. Tashlitsky, A. M. Arutyunyan, A.M. Kopylov, Putative mechanisms underlying high inhibitory activities of bimodular DNA aptamers to thrombin, Biomolecules 9 (2019) 41, https://doi.org/10.3390/biom9020041.
[53] L.A. Marky, K.J. Breslauer, Calculating thermodynamic data for transitions of any molecularity from equilibrium melting curves, Biopolymers 26 (1987) 1601–1620, https://doi.org/10.1002/bip.360260911.
[54] J.L. Mergny, L. Lacroix, Analysis of thermal melting curves, Oligonucleotides 13 (2003) 515–537, https://doi.org/10.1089/154545703322860825.
[55] L. Martino, A. Virno, A. Randazzo, A. Virgilio, V. Esposito, C. Giancola, M. Bucci, G. Cirino, L. Mayol, A new modified thrombin binding aptamer containing a 5′-5′ inversion of polarity site, Nucleic Acids Res. 34 (2006) 6653–6662, https://doi.org/10.1093/nar/gkl915.
[56] A. Virno, A. Randazzo, C. Giancola, M. Bucci, G. Cirino, L. Mayol, A novel thrombin binding aptamer containing a G-LNA residue, Bioorg. Med. Chem. 15 (2007) 5710–5718, https://doi.org/10.1016/j.bmc.2007.06.008.
[57] A. Virgilio, L. Petraccone, V. Vellecco, M. Bucci, M. Varra, C. Irace, R. Santamaria, A. Pepe, L. Mayol, V. Esposito, A. Galeone, Site-specific replacement of the thymine methyl group by fluorine in thrombin binding aptamer significantly improves structural stability and anticoagulant activity, Nucleic Acids Res. 43 (2015) 10602–10611, https://doi.org/10.1093/nar/gkv1224.
[58] L. Petraccone, E. Erra, L. Nasti, A. Galeone, A. Randazzo, L. Mayol, G. Barone, C. Giancola, Effect of a modified thymine on the structure and stability of [d(TGGGT)]4 quadruplex, Int. J. Biol. Macromol. 31 (2003) 131–137, https://doi.org/10.1016/S0141-8130(02)00073-9.
[59] L. Petraccone, E. Erra, V. Esposito, A. Randazzo, L. Mayol, L. Nasti, G. Barone, C. Giancola, Stability and structure of telomeric DNA sequences forming quadruplexes containing four G-tetrads with different topological arrangements, Biochemistry 43 (2004) 4877–4884, https://doi.org/10.1021/bi0300985.
[60] C.M. Olsen, W.H. Gmeiner, L.A. Marky, Unfolding of G-quadruplexes: energetic, and ion and water contributions of G-quartet stacking, J. Phys. Chem. B 110 (2006) 6962–6969, https://doi.org/10.1021/jp0574697.
[61] L. Petraccone, C. Spink, J.O. Trent, N.C. Garbett, C.S. Mekmaysy, C. Giancola, J. B. Chaires, Structure and stability of higher-order human telomeric quadruplexes, J. Am. Chem. Soc. 133 (2011) 20951–20961, https://doi.org/10.1021/ja209192a.
[62] C. Riccardi, D. Musumeci, I. Russo Krauss, M. Piccolo, C. Irace, L. Paduano, D. Montesarchio, Exploring the conformational behaviour and aggregation properties of lipid-conjugated AS1411 aptamers, Int. J. Biol. Macromol. 118 (2018) 1384–1399, https://doi.org/10.1016/j.ijbiomac.2018.06.137.
[63] F. Moccia, C. Riccardi, D. Musumeci, S. Leone, R. Oliva, L. Petraccone, D. Montesarchio, Insights into the G-rich VEGF-binding aptamer V7t1: when two G-quadruplexes are better than one!, Nucleic Acids Res. 47 (2019) 8318–8331, https://doi.org/10.1093/nar/gkz589.
[64] E. Napolitano, C. Riccardi, R. Gaglione, A. Arciello, V. Pirota, A. Triveri, F. Doria, D. Musumeci, D. Montesarchio, Selective light-up of dimeric G-quadruplex forming aptamers for efficient VEGF165 detection, Int. J. Biol. Macromol. 224 (2023) 344–357, https://doi.org/10.1016/j.ijbiomac.2022.10.128.
[65] H. Dougan, D.M. Lyster, C.V. Vo, A. Stafford, J.I. Weitz, J.B. Hobbs, Extending the lifetime of anticoagulant oligodeoxynucleotide aptamers in blood, Nucl. Med. Biol. 27 (2000) 289–297, https://doi.org/10.1016/S0969-8051(99)00103-1.
[66] S. Uehara, N. Shimada, Y. Takeda, Y. Koyama, Y. Takei, H. Ando, S. Satoh, A. Uno, K. Sakurai, 3′ poly(dA)-tailed thrombin DNA aptamer to increase DNase-resistance and clotting inhibitory activity, Bull. Chem. Soc. Jpn 81 (2008) 1485–1491, https://doi.org/10.1246/bcsj.81.1485.
[67] Y. Kasahara, S. Kitadume, K. Morihiro, M. Kuwahara, H. Ozaki, H. Sawai, T. Imanishi, S. Obika, Effect of 3′-end capping of aptamer with various 2′,4′-bridged nucleotides: enzymatic post-modification toward a practical use of polyclonal aptamers, Bioorg. Med. Chem. 20 (2010) 1626–1629, https://doi.org/10.1016/j.bmcl.2010.01.028.
[68] C. Riccardi, I. Russo Krauss, D. Musumeci, F. Morvan, A. Meyer, J.J. Vasseur, L. Paduano, D. Montesarchio, Fluorescent thrombin binding aptamer-tagged nanoparticles for an efficient and reversible control of thrombin activity, ACS Appl. Mater. Interfaces. 9 (2017) 35574–35587, https://doi.org/10.1021/acsami.7b11195.
[69] G.D. Hoke, K. Draper, S.M. Freier, C. Gonzalez, V.B. Driver, M.C. Zounes, D. J. Ecker, Effects of phosphorothioate capping on antisense oligonucleotide stability, hybridization and antiviral efficacy versus herpes simplex virus infection, Nucleic Acids Res. 19 (1991) 5743–5748, https://doi.org/10.1093/nar/19.20.5743.
[70] L.C. Bock, L.C. Griffin, J.A. Latham, E.H. Vermaas, J.J. Toole, Selection of single-stranded DNA molecules that bind and inhibit human thrombin, Nature 355 (1992) 564–566, https://doi.org/10.1038/355564a0.
[71] I. Smirnov, R.H. Shafer, Effect of Loop Sequence and Size on DNA Aptamer Stability, Biochemistry 39 (2000) 1462–1468.
[72] V.B. Tsvetkov, A.M. Varizhuk, G.E. Pozmogova, I.P. Smirnov, N.A. Kolganova, E. N. Timofeev, A universal base in a specific role: tuning up a thrombin aptamer with 5-nitroindole, Sci. Rep. 5 (2015) 16337, https://doi.org/10.1038/srep16337.
[73] W.A. Kibbe, OligoCalc: an online oligonucleotide properties calculator, Nucleic Acids Res. 35 (2007) 43–46, https://doi.org/10.1093/nar/gkm234.
[74] L. Petraccone, B. Pagano, C. Giancola, Studying the effect of crowding and dehydration on DNA G-quadruplexes, Methods 57 (2012) 76–83, https://doi.org/10.1016/j.ymeth.2012.02.011.
[75] C. Riccardi, A. Meyer, J.J. Vasseur, D. Cavasso, I. Russo Krauss, L. Paduano, F. Morvan, D. Montesarchio, Design, synthesis and characterization of cyclic NU172 analogues: a biophysical and biological insight, Int. J. Mol. Sci. 21 (2020) 3860, https://doi.org/10.3390/ijms21113860.
[76] M. Petersheim, D.H. Turner, Base-stacking and base-pairing contributions to helix stability: thermodynamics of double-helix formation with CCGG, CCGGp, CCGGAp, ACCGGp, CCGGUp, and ACCGGUp, Biochemistry 22 (1983) 256–263, https://doi.org/10.1021/bi00271a004.
[77] C. Riccardi, D. Musumeci, C. Platella, R. Gaglione, A. Arciello, D. Montesarchio, Tuning the polymorphism of the anti-VEGF G-rich V7t1 aptamer by covalent dimeric constructs, Int. J. Mol. Sci. 21 (2020) 1963, https://doi.org/10.3390/ijms21061963.
[78] C. Riccardi, F. D'Aria, F.A. Digilio, M.R. Carillo, J. Amato, D. Fasano, L. De Rosa, S. Paladino, M.A.B. Melone, D. Montesarchio, C. Giancola, Fighting the Huntington's disease with a G-quadruplex- forming aptamer specifically binding to mutant huntingtin protein: biophysical characterization, in vitro and in vivo studies, Int. J. Mol. Sci. 23 (2022) 4804, https://doi.org/10.3390/ijms23094804.
[79] C. Riccardi, F. D'Aria, D. Fasano, F.A. Digilio, M.R. Carillo, J. Amato, L. De Rosa, S. Paladino, M.A.B. Melone, D. Montesarchio, C. Giancola, Truncated analogues of a G-quadruplex-forming aptamer targeting mutant huntingtin: shorter is better!, Int. J. Mol. Sci. 23 (2022) 12412, https://doi.org/10.3390/ijms232012412.
[80] R. De Cristofaro, E. Di Cera, Phenomenological analysis of the clotting curve, J. Protein Chem. 10 (1991) 455–468, https://doi.org/10.1007/BF01025473.
[81] M. De Fenza, E. Eremeeva, R. Troisi, A. Esposito, F. Sica, P. Herdewijn, D. D'Alonzo, A. Guaragna, Structure-activity relationship study of a potent α-thrombin binding aptamer incorporating hexitol nucleotides, Chem. Eur. J. 26 (2020) 9589–9597, https://doi.org/10.1002/chem.202001504.